THE OLD POTTER'S ALMANACK

Volume Twenty-four, Number One: June 2022. ISSN 0965-7479

EDITORIAL

Dear Reader,

The *Old Potter's Almanack* was paused for the last two years due to a series of events, included the dreadful Covid pandemic, that, among the tragic events, also slowed down a variety of research activities.
This issue presents three papers. In the first, Jasna Vuković discusses the role of Neolithic black-topped ceramics with a polychrome effect at the Serbian site of Pavlovac-Čukar, which as well as showing traces of use, were often repaired and reused.

In the second paper, Cristian Eduard Ştefan describes an intriguing pot, an *askos*, found at the Boian site of Radovanu-La Muscalu in Romania. Ştefan suggests that this vessel type had probably a functional role, and provides us with an overview on similar finds from the Gumelniţa-Karanovo VI area.

In the third paper, Nigel Meeks and Michael Tite offer a detailed description on the use of high-resolution SEM-EDX elemental X-ray maps and colour optical microscopy images to study ceramic phases, focusing on their application to maiolica body and glaze. This is a much-needed paper for all colleagues who use the SEM-EDX analytical tool.

I am deeply saddened to let you know that Dr Roberta Tomber, whom many of you knew as an amazing researcher, original thinker, enthusiastic and excellent archaeologist and petrographer, sadly passed away on the 1st of May. Since the initial phases of the CPG, Roberta has been key to it and was one of the most serious, supportive and appreciated scholars, and one of my dearest friends. I recently worked with Roberta on co-editing a special issue of the *Journal of Archaeological Science: Reports* (https://www.sciencedirect.com/journal/journal-of-archaeological-science-reports/vol/16/suppl/C). She was incredibly clever, careful, with an eagle eye for detail, and extremely fun to work with. This issue includes an obituary for Roberta, to offer a glimpse into her incredibly productive and rich life.

Michela Spataro

IN THIS ISSUE

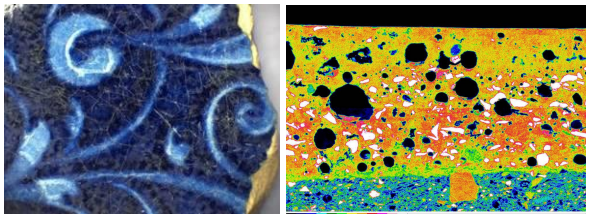

REPAIR AND CURATION OF LATE NEOLITHIC THREE-COLOURED POTS: INSIGHTS FROM THE SITE OF PAVLOVAC-ČUKAR, SOUTHERN SERBIA

Jasna Vuković

Department of Archaeology, Faculty of Philosophy
University of Belgrade, Serbia
E-mail: jvukovic@f.bg.ac.rs

Three-coloured vessels, usually called *black-topped* pottery, are widely known from a vast geographical area (from Egypt and Sudan, the Near East, the Balkans, and even India) and from a wide chronological span – from the Neolithic to the Protohistorical periods. Despite several experiments (Hendrickx *et al.* 2000; Bintintan and Gligor 2018; Vuković 2018a), the technology, i.e. firing procedure, is still to a great extent unknown. However, researchers agree that these vessels were fired in a combined atmosphere, where some parts of the pots were exposed to oxidising conditions, while other parts were (assumed to be) pressed into the ashes or wrapped in wet leaves during firing, in order to achieve blackening of the surface in a reducing atmosphere. On the other hand, firing installations are still unknown: some researchers assume the presence of kilns (Hendrickx *et al.* 2000; Bintintan and Gligor 2018), despite the absence of such structures in the archaeological record, while others consider the use of a bonfire as a more probable solution (Bonga 2013; Kalogirou 1994; Vuković 2018a).

Black-topped pots are one the most remarkable features of the earliest phases of the Late Neolithic Vinča culture of the Central Balkans (Garašanin 1979). They include bowls, and more often pedestalled vessels usually called 'goblets'. In contrast to bichrome (black and red) black-topped vessels from modern Bulgaria and Greece, they exhibit three colours: a black upper part, a yellowish-beige central part, and a red lower part. The different coloured zones on the pots are usually distinctly divided, with clear horizontal margins (Figure 1). The central, yellowish-beige zone of the pots, being regular and in clearly defined bands, does not appear to be the consequence of combined firing conditions, as has been suggested (Kalogirou 1994, 88), but it was more probably executed deliberately. Moreover, lower, yellow and red parts of the pots were slipped.

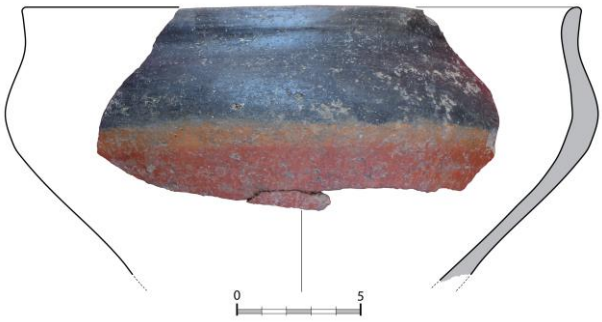

Figure 1. The different coloured zones on the pots are usually distinctly divided, with clear horizontal margins.

The use of coating of iron-rich clay on Vinča pots is already confirmed (Spataro 2018). Although the effect of the slip coating in producing a polychrome effect has not yet been experimentally tested, it can be assumed that clear horizontal boundaries between the zones of different colours may have been the result of the coating application, thus achieving a better control over their distribution.

During the rescue excavations at the site of Pavlovac-Čukar (Figure 2) in southern Serbia in 2011, several specimens of three-coloured black-topped vessels were found. In most cases, they were found in surface layers, disturbed by modern agricultural activities. Although information about archaeological context is lacking, the ancient modifications of these pots may shed some light on their function and meaning.

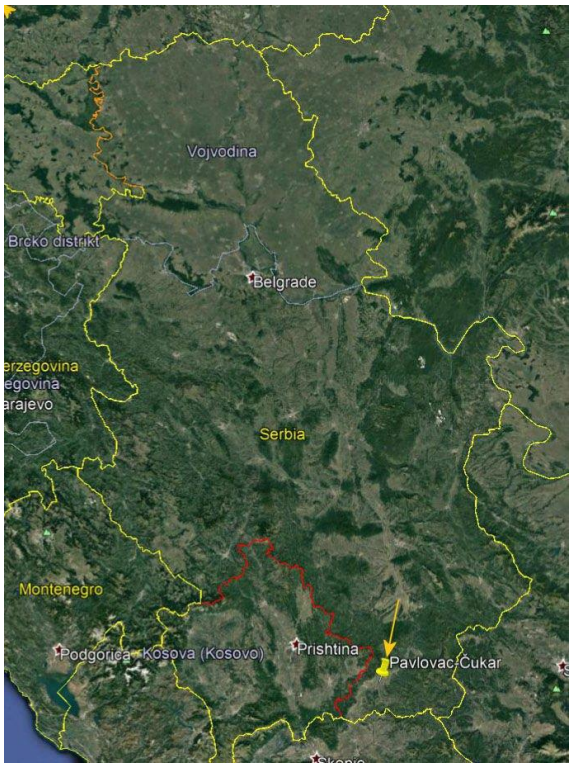

Figure 2. Site of Pavlovac-Čukar, arrowed.

Black-topped Vinča vessels usually exhibit well-preserved surfaces. Traces of use such as notches, incisions or any other form of abrasion or mechanical damage, as well as other kinds of use-alterations (surface spalling, non-abrasive attrition, accretions etc.), are generally absent. The only exception is abrasion of the base, which often occurs as a consequence of frequent handling and usage. However, the Pavlovac-Čukar black-topped pots exhibit different kinds of modifications, such as curation and repair.

The fragment shown in Figure 3 is the lower part of a pedestalled vessel. Its 'bottom' was completely flattened, but not as a consequence of use. The whole of this surface was uniformly abraded. As the mineral temper does not protrude from the surface (it is not 'pedestalled')[1], the base must have been abraded with something harder than the ceramic, probably an abrasive stone tool (cf. Vuković 2017a); thus, the whole bottom represents the zone on which a continuous repetition of the abrasive process occurred (Schiffer and Skibo 1989). The original fired surface of the base was completely removed, revealing the cross-section of the base, allowing us to make significant observations about the technology. The colours on the cross-section, red on the exterior with blurred margin in relation to the inner dark grey colour indicate oxidised firing.

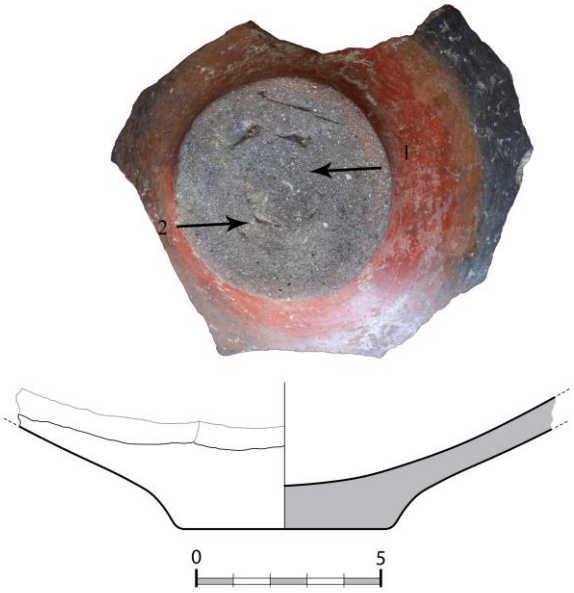

Figure 3. The lower part of a pedestalled vessel. Its 'bottom' was completely flattened.

The central 'cylinder' with a layer of clay around it, clearly indicates that this vessel had a foot (pedestal); when it broke, the broken edge remaining on the base of the pot was flattened, extending the use of the pot. Similar intervention was observed on the specimen in Figure 4: the foot (pedestal) of the pot, which must have been broken or chipped and have become unstable, was flattened in the same manner, using an abrasive (stone) tool.

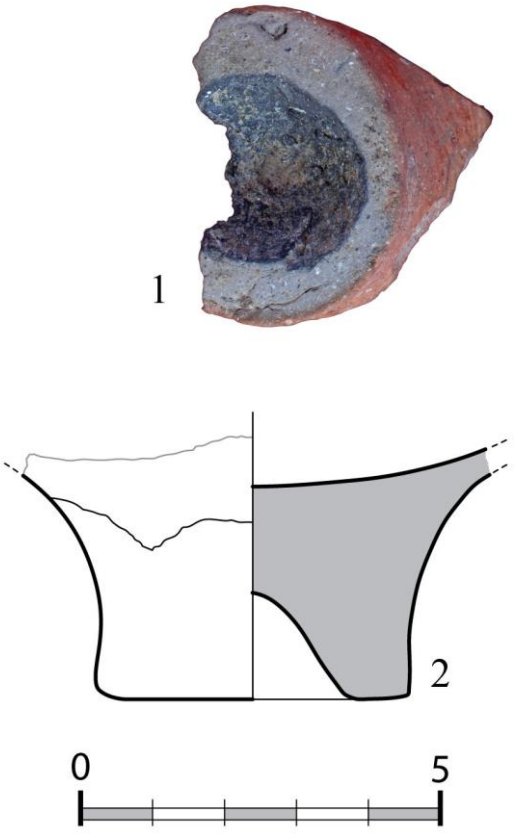

Figure 4. 1. Underside of vessel showing the flattened standing surface of the broken pedestal. The foot of the pot was flattened using an abrasive (stone) tool.

Ancient repair/modifications were seen on two broken foot (pedestal) fragments (Figures 5 and 6). These have a red-slipped exterior and a black interior surface, with traces of a tool used in the process of surface scraping/thinning during the forming of the vessel.

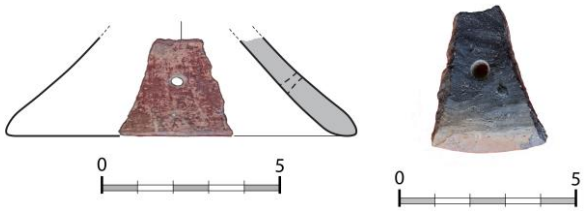

Figure 5. Foot (pedestal) fragment with perforation. Obverse and reverse sides.

In both cases, single perforations are present. These were executed after the firing, slightly above the foot-rim. The hole shown as an example in Figure 5 exhibits chipped edges, indicating that the hole was drilled from the exterior. The other specimen lacks

[1] See Schiffer and Skibo (1989) using "pedestalled temper" as a consequence of contact with soft abrader.

these kinds of traces. Modifications in the form of drilled holes are usually interpreted as repairs: by using some kind of strings, two broken pieces of a pot could be joined and used further.

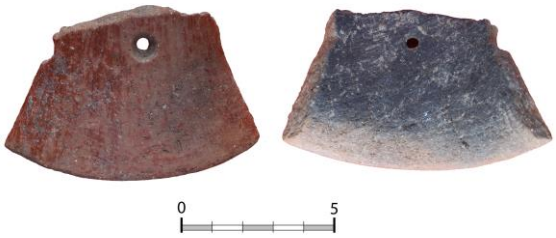

Figure 6. Foot (pedestal) fragment with perforation. Obverse and reverse sides.

One fragment of a vessel foot (Figure 7) differs from the previously described specimens in several important features. Undoubtedly, it belongs to the group of Vinča pedestalled vessels, with a red-slipped exterior and a black interior surface.

Figure 7. Fragment of a vessel pedestal differs from the previous specimens in several important features.

However, its fabric is different. While the other specimens were made of a fine fabric with mineral inclusions and with no macroscopically visible organic matter, this specimen is rich in organic temper. Moreover, the black core is visible in the cross-section. This could be another example of technological hybrid between two Neolithic traditions – Starčevo and Vinča, already confirmed on the ceramics from the site of Pavlovac-Čukar (Vuković 2017b). The modification on this vessel is not, however, a repair, nor a curation, but rather the change of a vessel function. On the bottom of the pot, a hole with a diameter of *ca.* 1 cm was pierced from the interior (Figure 7). The edges of the hole are rounded, indicating liquid abrader, i.e. abrasion caused by a continuous contact of the ceramics with water or some other liquid. Similar examples are known from several Early Neolithic sites, e.g. at Donja Branjevina (see Karmanski 2005, T. CXI/1), as well as from the site of Čukar (Vuković 2018b).

The concept of value of ceramic pots could be considered through the analysis of repairs, and the considerations of breakage and replacement rates. In other words, the vessel will need to be repaired if a new vessel is not available. According to research (Senior 1995; Dooijes and Nieuwenhuyse 2009), the most commonly repaired vessels are those with special importance to their users; these are often luxury vessels, used on special occasions. The most commonly recorded repairs in ceramic assemblages from a wide chronological span are perforations, i.e. 'repair holes', positioned along the fractures of the fragments, which were connected by some thread, or wire in later periods (Dooijes and Nieuwenhuyse 2009; Vuković 2017c, 179-180). Repair holes were recorded in Vinča black-topped pottery from the beginning of research at Vinča-Belo Brdo (Vasić 1936, 18): they were interpreted as evidence that this kind of pottery was highly valuable. It is usually considered that hole drilling may cause the change of vessel function. This is especially true when the holes were drilled in the vessel wall: if a binding agent was not used[2], then leakage of the contents could easily occur. However, modification of vessel feet should not cause a change in function since the holes are not drilled through the walls of the vessel. Therefore, these modifications were not conditioned by strictly functional requirements, and may indicate a different, not strictly utilitarian function of black-topped pottery. The flattened bases of pedestalled vessels can also be regarded in the same way.

The special role or value of black-topped pottery can also be inferred from the technological process. Combined, oxidised-reduced firing atmosphere is time-consuming, and requires special knowledge, skill, experience and expertise of the potter. According to some estimates, however, black-topped pottery was produced in very low quantities (Bonga 2013). This is supported by the fact that black-topped pots are quite rare in Vinča assemblages, indicating limited production and the possibility that they were made only for special occasions. It could further be hypothesised that they were not available to all members of the community and every household.

All these observations indicate that repairs on the black-topped pots, that enabled their extended use, were not conducted for strictly functional reasons. Furthermore, their low frequencies in assemblages, the absence of use-wear traces, and complex technological process, suggest their special purpose. Whether they had a role of prestigious, ritual, or high-status items is still unclear.

[2] In the case of black-topped pottery in Neolithic Greece, archaeometric analyses revealed the usage of binding agents, such as birch-bark tar (Urem-Kotsou *et al.* 2002).

References

Bintintan, A. and Gligor, M. 2018. Pottery kiln: A technological approach to Early Eneolithic black-topped production in Transylvania. *Studia Antiqua et Archaeologica* 22 (1), 5-18.

Bonga, L. A. 2013. *Late Neolithic Pottery from Mainland Greece, ca. 5,300-4,300 B.C.* PhD thesis. Philadelphia: The Temple University.

Dooijes, R. and Nieuwenheyse, O. 2009. Ancient repairs in archaeological research: a Near Eastern perspective. In Ambers, J., Higgitt, C., Harrison, L. and Saunders, D. (eds.), *Holding It All Together: Ancient and Modern Approaches to Joining, Repair and Consolidation*, 8–12. Archetype Publications. London.

Garašanin, M. 1979. Centralnobalkanska zona. In: *Praistorija jugoslavenskih zemalja* II, urednik Alojz Benac, Sarajevo: Svijetlost i Akademija nauka i umjetnosti Bosne i Hercegovine, 79-212.

Hendrickx, S., Friedman, R. and Loyens, F. 2000. Experimental Archaeology concerning Black-Topped Pottery from Ancient Egypt and the Sudan. *Cahiers de le Céramique Egyptienne* 6, 171-187.

Kalogirou, A. 1994. *Production and consumption of pottery in Kitrini Limni, West Macedonia, Greece, 4500 B.C.-3500 B.C.*, unpublished PhD thesis. Ann Arbor, Indiana University.

Karmanski, S. 2005. *Donja Branjevina: A Neolithic Settlement near Deronje in the Vojvodina (Serbia).* Edited by P. Biagi. Atti della Società per la Preistoria e Protostoria della Regione Friuli-Venezia Giulia, Quaderno 10. Trieste.

Schiffer, M. B. and Skibo, J. M. 1989. A Provisional Theory of Ceramic Abrasion. *American Anthropologist* 91(1), 101–115.

Senior, L. M. 1995. The Estimation of Prehistoric Values: Cracked Pot Ideas in Archaeology. In Skibo, J. M., Walker, W. H., and Nielsen, A. E (eds.), *Expanding Archaeology*. Salt Lake City: University of Utah Press, 92–110.

Spataro, M. 2018. Origins of specialization: The ceramic chaîne opératoire and technological take-off at Vinča-Belo Brdo, Serbia. *Oxford Journal of Archaeology* 37(3), 247–265.

Urem-Kotsou, D., Stern, B., Heron, C. and Kotsakis, K. 2002. Birch-tar at Neolithic Makriyalos, Greece. *Antiquity* 76, 962–967.

Vasić, M. 1936. *Preistoriska Vinča* III, Beograd: Izdanje i štampa Držane štamparije Kraljevine Jugoslavije.

Vuković, J. 2017a. Popravke i produžena upotreba keramičkih posuda: primer ranoneolitske zdele s Kovačkih Njiva (Repairs and extended use of ceramic vessels: An Early Neolithic bowl from Kovačke njive). *Zbornik Narodnog muzeja* XXIII-1, 123-133.

Vuković, J. 2017b. Erasing boundaries or changing identities? The transition from Early/Middle to Late Neolithic, new evidence from Southern Serbia. In Gori, M. and Ivanova, M. (eds.) *Balkan dialogues: Negotiating Identity between Prehistory and the Present*, 240-253. Routledge. London.

Vuković, J. 2017c. *Studije keramike: Teorija i metodologija u analizama grnčarije u arheologiji*. Beograd: Zavod za udžbenike.

Vuković, J. 2018a. Late Neolithic Vinča pottery firing procedure: Reconstruction of Neolithic technology through experiment. *Opuscula Archaeologica* 39/40, 25-35.

Vuković, J. 2018b. Neolithic painted pottery: A Case study from Pavlovac-Čukar, Southern Serbia. *From Crafts to Art: Ceramics. Technology, decor, style*, Internationa Academic Research Conference, St. Petersburg, 22-25 May 2018, abstracts, Sankt Petersburg: Saint Petersburg Stieglitz State Academy of Art and Design, State Hermitage Museum, Institute of History of Material Culture RAS, 29-30.

AN *ASKOS*-TYPE VESSEL FROM RADOVANU-*LA MUSCALU*, ROMANIA

Cristian Eduard Ştefan

"Vasile Pârvan" Institute of Archaeology, Romanian Academy, Henri Coandă str., No. 11, Bucharest
E-mail: cristarh_1978@yahoo.com

Introduction

The archaeologist Eugen Comşa researched the Chalcolithic settlement of Radovanu-*La Muscalu,* Călăraşi County, in southern Romania for over 30 years (1960-1990), producing impressive results (Comşa 1974; 1990). The main settlement is marked by a short occupation of the Vidra phase and four evolving stages of the Spanţov phase of the Boian culture (5200-4550 cal. BC). Radovanu-*La Muscalu* is in fact an assemblage consisting of a settlement positioned on a high terrace, a second one eastward at the foot of the hill, a weaving workshop and the necropolis both situated westward (Figures1 and 2).

Figure 1. The topographic position of the settlement at Radovanu-La Muscalu, Romania (Google Earth).

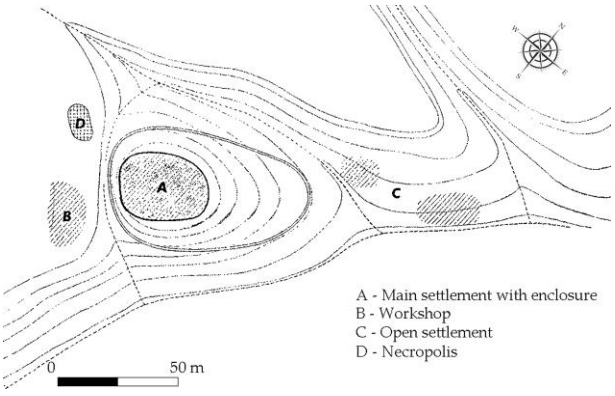

Figure 2. The settlement at Radovanu-La Muscalu (after Comşa 1990, modified).

The excavation of this settlement yielded rich archaeological material comprising pottery, figurines, miniaturist models of dwelling units, flint, bone and antler tools, and jewellery, mostly still unpublished and currently under study. Within the framework of this re-examination of the material from this important site, a particular focus has been to address the study of aspects concerning pottery making traditions at Radovanu (Ştefan 2019, 144-155).

During the excavations, a large amount of pottery was collected (roughly estimated to 15,000 fragments), most of which remains unpublished. The assemblage includes footed vessels, 'amphorae', bowls, lids, storage vessels, cups, box-shaped stands, beakers, jars or strainers. A diverse range of shapes includes three main categories of fabric, identified according to their coarseness: fine, intermediate and coarse. The main decoration styles consisted of incisions, excision and filling with white paste, channelling, graphite painting, red ochre painting or plastic applications (Comşa 1990, 51-67).

Description of the vessel

In this contribution we analyse a special type of vessel coined as *askos* in the literature. The item was defined as a "*vessel, originally shaped like a leather bottle (uter) for holding water or wine. It was furnished with a handle at the top, and had sometimes two mouths, one which served to fill, the other to empty it. Later on, the askos assumed the form of an earthenware pitcher*" (Mollett 1996, 26; see also the discussion in Marinescu-Bîlcu 1990, 5).

The vessel was discovered in the last habitation layer of the settlement at Radovanu-*La Muscalu*. This layer could be dated in absolute chronology sometime in the middle of the 5th millennium BC towards the final stage of the Spanţov phase of Boian culture. Unfortunately, the precise context of the vessel is unknown, aside from the label "Layer 1". The fact that it was found almost complete could suggest an activity area or maybe was covered by the crumbling walls of a burnt dwelling in the external part of the structure.

The vessel was not decorated and its surface was burnished inside and outside; the firing evidence shows a reducing atmosphere, the fabric is semi-fine and it was tempered with grog[3]. The vessel colour is brown-greyish and in the extension of the handle shows an embossed plastic application that ends with a short tail, the whole assembly suggesting a stylised bovine. Seen from above, the *askos* is slightly domed on the sides, while the base is perfectly flat and

[3] Grog was here determined by macroscopic examination.

shows signs of friction, most likely due to the heavy use of the container.

The vessel dimensions are the following: mouth diameter – 9 cm, base maximum length – 18.5 cm, base maximum width – 11.5 cm, maximum height – 13.7 cm, capacity – *ca.* 1350 ml (Figures 3 and 4).

Figure 3. The askos vessel from Radovanu-La Muscalu (photo C.E. Ştefan).

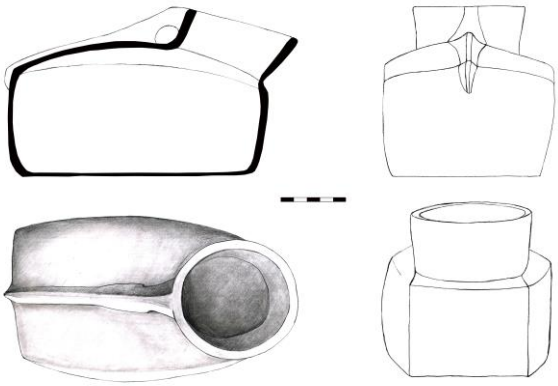

Figure 4. The askos vessel from Radovanu-La Muscalu (drawing C. Georgescu).

Discussion

The closest analogies for this vessel can be seen in the settlements of Mălăieştii de Jos (Paveleţ 2010, Fig. 16/1) and Seciu (Frînculeasa 2011, Pl. 36/3), both in Prahova County and belonging to the Stoicani-Aldeni cultural aspect (Figures 5 and 6). This cultural aspect was defined as a mix between Cucuteni-Ariuşd and Gumelniţa cultures, its position and material culture suggest a buffer zone (Dragomir 1983). Both settlements mentioned above benefitted from radiocarbon dates which are synchronous between *ca.* 4340-4220 cal BC (Frînculeasa 2016, 68-69, Tab. 1, Fig. 4). Vessels of this type were previously known in the Stoicani-Aldeni area at Vulcăneşti, Suceveni, Dodeşti or Sudiţi (Dragomir 1983, 165, Figs. 41/5, 6; 45/2; Paveleţ and Grigoraş 2011, 23, Fig. 61/6).

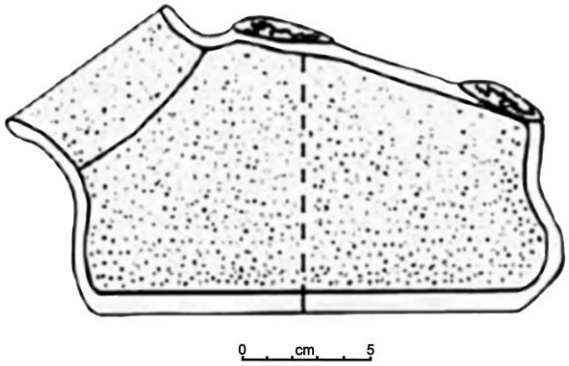

Figure 5. The askos vessel from Mălăieştii de Jos (after Paveleţ 2010).

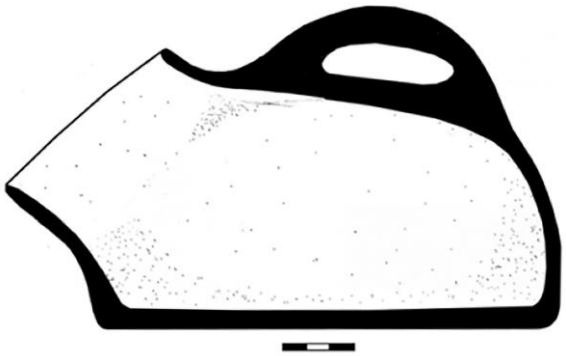

Figure 6. The askos vessel from Seciu (after Frînculeasa 2011).

Other vessels of this type were discovered in Gumelniţa-Karanovo VI and Sălcuţa-Krivodol areas, showing different shapes, sizes and decorations (Figure 7). The oldest *askoi* of Căscioarele belonged to A2 phase of the Gumelniţa culture (Marinescu-Bîlcu 1990, 6; Voinea 2005, 46-47, Pl. 97), which is dated between 4450-4250 cal BC in Greater Wallachia (Bem 2001, 43). On the other hand, *askos* type vessels were discovered in earlier contexts south of the Danube, such as those attributed to the Marica culture, which is roughly contemporaneous with Boian at the north of the Danube (Todorova 1986, 99, Fig. 23/6).

In general, these vessels were discovered in domestic contexts, either in dwellings amongst debris, or in the habitation layer, possibly indicating some activity

areas. A special case was that of the Mălăieşti *askos*. The vessel was found amongst the debris of a burnt dwelling (dwelling no. 5) and a fragmentary flat bone figurine and an animal bone were found inside it, which led to the hypothesis that the *askos* was used in some sort of cultic ceremonies (Paveleţ 2010, 39).

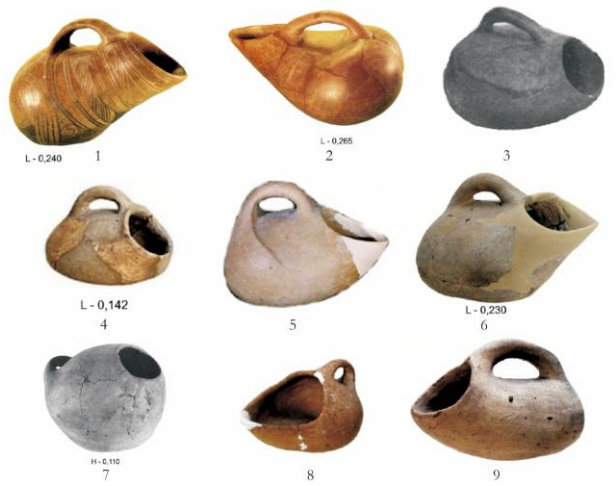

Figure 7. Askos type vessels from Gumelniţa-Karanovo VI area (after Voinea 2005, different scales).

The capacity of the vessels from Căscioarele, is quite different, 150 ml, 250 ml, 1400 ml and 1800 ml respectively, which ruled out from the starting point any hypothesis concerning a possible unit (Marinescu-Bîlcu 1990, 6). According to Marinescu-Bîlcu their role was not cultic, rather practical: either large spoons for pouring flour or grains, either containers for serving or storing liquids (Marinescu-Bîlcu 1990, 16). On the other hand, we know the spectacular anthropomorphic figurine from Liubcova-*Orniţa* with a mask in one hand and a vessel in the other. The pot was interpreted as an *askos*, so the figurine represented and individual that was involved in some kind of ceremony (Luca 1989, 229-234; Schier 2005, 71, no. cat. 25). A second anthropomorphic figurine discovered later in the same settlement has also an *askos* type vessel represented on the belly, the item being interpreted as proving the libation act in ceremonies related to the cult of fertility and fecundity (Luca 2002, 18-20, Fig. 1, Photo 1, 2).

It is interesting to note that first definitions of the *askos* type vessels from dictionaries and lexicons are linked with animals: either they relate explicitly to animal leather, or are defined as "duck-shaped vessels" (Marinescu-Bîlcu 1990, 5). If we take a closer look at the Radovanu-*La Muscalu* vessel, we can observe that it could represent a very stylised ox or bull. The withers line is obvious on the upper side of the vessel and we can see also a short tail at the end. This fact can strengthen the animal body/clay vessel metaphor which we tried to analyse a few years ago with some Vinča materials from Şoimuş-*La Avicola (Ferma 2)*, Hunedoara County (Ştefan 2014, 14-22; Ştefan *et al.* 2015, 183-209).

Conclusions

Sometime in the middle of the 5th millennium BC a new vessel shape emerged in the Lower Danube, a shape that survived somehow until the Classical Period of Greece. Most probably it was used for transporting, serving and storing liquids, having as a model some prototypes made of animal leather. This fact is strengthened by the burnished surface (interior and exterior) of some of the *askoi*, which is very useful in reducing the walls porosity and better preventing the evaporation of liquids.

The practical and cultic role of such vessels are not mutually exclusive. Although they are mainly found in domestic contexts, they could have been used in ceremonies whose significance escapes us today; this thought is suggested by artifacts such as the anthropomorphic figurines from Liubcova-*Orniţa* (Lazarovici and Lazarovici 2006, 505-506).

A better conclusion is the paragraph of a well-known professor after years of experience in the field: "…*the question is not so much to determine where function stops and symbol (or style) begins, but to be aware of their remarkable intricacy. Indeed, making pottery and 'making sense' are two compatible, entangled, and above all, complementary processes*" (Gosselain 1999, 221).

References

Bem, C. 2001. Noi propuneri pentru o schiţă cronologică a eneoliticului românesc. *PONTICA* XXXIII-XXXIV, 25-121.

Comşa, E. 1974. *Istoria comunităţilor culturii Boian,* Bucarest.

Comşa, E. 1990. Complexul neolitic de la Radovanu. *Cultură şi Civilizaţie la Dunărea de Jos* VIII, 5-126.

Dragomir, I. T. 1983. *Eneoliticul din sud-estul României. Aspectul cultural Stoicani-Aldeni.* Bucureşti.

Frînculeasa, A. 2011. *Seciu – judeţul Prahova, un sit din epoca neo-eneolitică în nordul Munteniei.* Ploieşti.

Frînculeasa, A. 2016. Nordul Munteniei şi cronologia aspectului cultural Stoicani-Aldeni – stratigrafie, elemente de reper şi date radiocarbon din situl

de la Mălăieştii de Jos (jud. Prahova). *Buletinul Muzeului Judeţean Teleorman* 8, 59-107.

Gosselain, O. 1999. In Pots we Trust: The processing of Clay and Symbols in Sub-Saharan Africa. *Journal of Material Culture* 4(2), 205-230.

Lazarovici, C. M, and Lazarovici, Gh. 2006. *Arhitectura Neoliticului şi Epocii Cuprului din România. I. Neoliticul*. Iaşi.

Luca, S. A. 1989. Die Statuette von Liubcova-Orniţa (Jud. Caraş-Severin). *DACIA N.S*. XXXIII, 229-234.

Luca, S. A. 2002. Date despre "statueta de la Liubcova II", jud. Caraş-Severin. *Acta Terrae Septemcastrensis* I, 15-28.

Marinescu-Bîlcu, S. 1990. Askoï et rhytons énéolithiques des régions balkano-danubiennes et leur relations avec le sud, à la lumière de quelques pièces de Căscioarele. *DACIA N.S*. XXXIV, 5-21.

Mollett, J. W. 1996. *Dictionary of Art and Archaeology*. London.

Paveleţ, E. 2010. *Ceramica Stoicani-Aldeni din aşezările de la Mălăieştii de Jos (jud. Prahova) şi Coţatcu (jud. Buzău)*. Ploieşti.

Paveleţ, E. and Grigoraş, L. 2011. *Ceramica Stoicani-Aldeni. Studiu de caz: tell-ul de la Aldeni, com. Cernăteşti, jud. Buzău*. Ploieşti.

Schier, W. 2005. *Katalog zur Sonderausstellung Masken, Menschen, Rituale. Alltag un Kult vor 7000 Jahren in der prähistorischen Siedlung von Uivar, Rumänien*. Würzburg.

Ştefan, C. E. 2014. Some special clay artifacts from Şoimuş-La Avicola (Ferma 2), Hunedoara County, Romania. *The Old Potter's Almanack* 19(2), 14-22.

Ştefan, C. E. 2019. Some Aspects Concerning Pottery Making at Radovanu-La Muscalu, Romania (first half of the 5th Millennium BC). In Amicone, S., Quinn, P.S., Marić, M., Mirković-Marić, N., Radivojević, M. (eds.) *Tracing Pottery-Making Recipes in the Prehistoric Balkans, 6th–4th Millennia BC*, 144-155. Oxford.

Ştefan, C. E., Petcu, R. and Petcu, Răz. 2015. Vase cu picioare de la Şoimuş-La Avicola (Ferma 2), jud. Hunedoara. *Studii şi cercetări de istorie veche şi arheologie* 66(3-4), 183-209.

Todorova, H. 1986. *Kamenno mednata epoha v Bulgariia: peto khiliadoletie predi novata era*. Sofia.

Voinea, V. 2005. *Ceramica complexului cultural Gumelniţa-Karanovo VI. Fazele A1 şi A2. Constanţa.*

THE APPLICATION OF HIGH-RESOLUTION SEM-EDX COMPOSITIONAL MAPPING TO THE TECHNOLOGICAL STUDY OF ANCIENT CERAMICS: A CASE STUDY ON ITALIAN MAIOLICA

Nigel Meeks[1] and **Michael Tite**[2]

[1] *Department of Scientific Research, The British Museum*
E-mail: nmeeks@britishmuseum.org

[2] *Emeritus Professor, University of Oxford, School of Archaeology*
E-mail: michael.tite@rlaha.ox.ac.uk

INTRODUCTION

The routine application of scanning electron microscopy with energy dispersive X-ray spectrometry (SEM-EDX) for high resolution mapping, analysis and imaging to the study of ancient ceramics is exemplified here by the study of 15th-17thC Italian Maiolica (see type in Figure 1 upper).

Figure 1. Upper: an example of maiolica Tondino dish with 'Berrettino' decoration, Faenza c. 1535/40 (image from web auction catalogue. Koller Auctions, 19 September 2016); lower: detail of the surface of a sherd (no 5) of similar pattern.

This ceramic material offers a complex mineralogical microstructure and chemistry within the coloured glaze on the fired ceramic bodies that epitomises the microanalytical approach used for the study and interpretation associated with the production technology, the raw materials used and the mineralogical changes that occur during glazing and firing. With the benefit of current high precision SEM-EDX instrumentation (Goldstein *et al.* 2003; 2018) it is timely to be reminded of the early paper by Freestone (1982), *Applications and potential of Electron Probe Micro-Analysis in technological and provenance investigations of ancient ceramics,* for which we hope this paper is complimentary to that early foresight.

In this paper, we illustrate the use of high-resolution X-ray compositional mapping (*ca.* 4100x2900 pixels) and associated backscattered electron (BSE) compositional images on one typical thick section of this type of complex microstructural glazed ceramic. The sample consisted of a polished section of a sherd (TW01[4]) from an early 16th century Italian maiolica plate (glaze and body) from Faenza with cobalt blue *berettino* decoration, similar to the sherd (sherd 5) shown in Figure 1 (lower).

Preliminary analytical data for the sherd (TW01) had previously been included in recent papers on the production technology of Italian maiolica (Tite 2009; 2012).

EXPERIMENTAL PROCEDURES

The maiolica sherd sample was mounted in cold-setting resin block 30mm diameter and 10mm deep and diamond polished to a very high finish, and optical micrographs taken (Figure 2a-c).

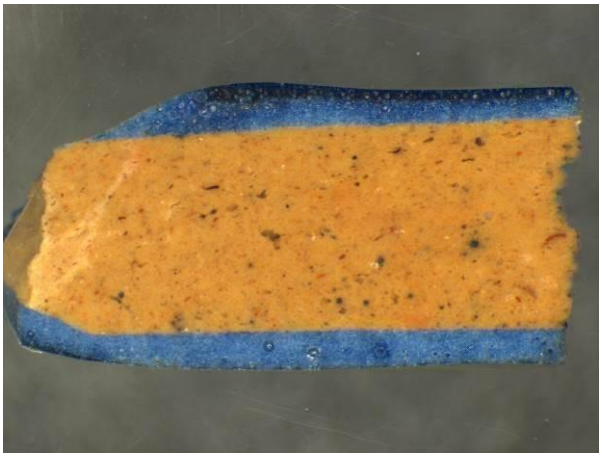

Figure 2a. Optical microscopy of the polished maiolica sample in the resin block.

[4] Professor Tim Wilson (ex-Ashmolean Museum) is thanked for providing sherd TW01.

b)

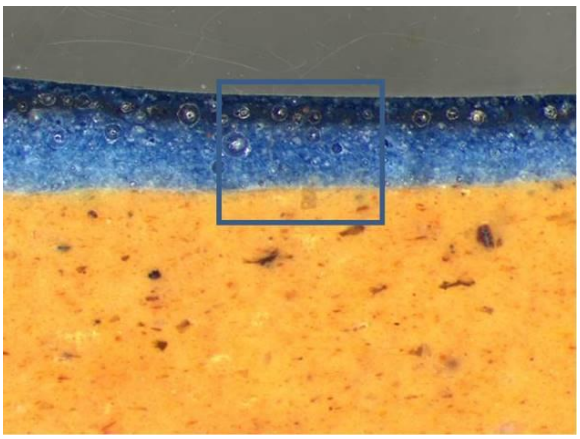

c)

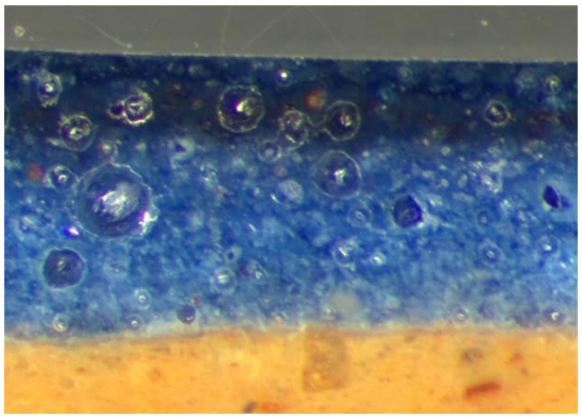

d)

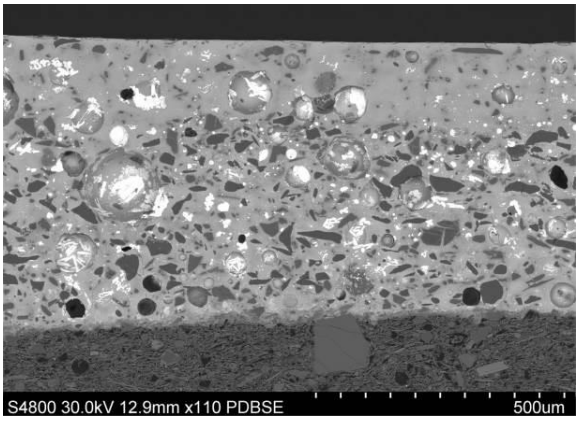

Figure 2 b), c). Optical microscopy of the polished maiolica sample in the resin block. Note the two layers of the blue glaze - the upper transparent deeper blue glaze and lower opaque glaze which appears lighter in colour due to tin oxide opacifier crystals. d) BSE image of the SEM-EDX map area showing the very complex mineralogy within the glazing.

The sample was vacuum coated with an extremely thin conducting layer of carbon for study in the high vacuum high-resolution SEM. The coating is not seen in the SEM under the operating conditions used.

The high-resolution study was carried out using an Oxford Instruments AZtec® EDX microanalysis system[5] run on an Hitachi S-4800FE field emission scanning electron microscope (FE-SEM) at the British Museum (London, United Kingdom). This combination provided two advantages - the very high-resolution digital X-ray mapping provided by the AZtec® microanalyser, *ca.* 4100 x 2900 pixels, combined with the high-resolution imaging capability of the FE-SEM at high magnification (Goldstein *et al.* 2017; Lyman *et al.* 1990). For imaging and analysis, the FE-SEM was run at 20kV which provided the best backscattered electron imaging for high contrast and low noise of the complex mineral and glassy phases in the ceramic sample (Meeks 1988). This is also the best kV to energise the full range of elements of interest for EDX analysis (Russ 2013, Statham 1998) of this maiolica, from the lighter ceramic matrix elements (O, Na, Mg, Al, Si, K, Ca), through the transition elements (Ti, Mn, Fe, Co, Ni) and up to the useful diagnostic high energy element lines of lead/arsenic/bismuth (*ca.* 10.5-13keV) on a spectrum range 0-20keV (Kortright and Thompson 2001[6]) The conditions provide efficient spectral collection at high count rate (*ca.* 9000cps with the particular analyser used) for X-ray elemental mapping and analysis. With such a large digital map image, *ca.*12 million map points, for which a full spectrum is obtained from each point, the time required for mapping is necessarily long, typically (overnight) for 16 hours, and the digital storage required is large (e.g. can be in the gigabyte range). The resulting map contains all elements of interest in the sum spectrum for the whole mapped area from which any, or all, detectable elements can be selected for reconstructing into elemental distribution maps.

The high-resolution BSE image of the mapped area allows very useful digital zoom for more detailed investigation of the complex microstructures, mineralogy and chemistry, without pixelation of the image or maps (see Figure 11). Selected areas can be made within the mapped area, for example on a high concentration element in an inclusion of interest, in which the associated pixel spectra are combined into a summed spectrum for that area which can be quantified.

RESULTS AND DISCUSSION

Body of the maiolica sample

The EDX analyses by Tite (2009, tables 1 and 3) of the ceramic body bulk composition (paste) of a number of Italian maiolica sherds include sample TW01. This sample is examined in detail here, as it is

[5] See Oxford Instruments Nanoanaysis *Application Notes.*
[6] See *X-ray Emission Energies.*

a typical of Italian maiolica of the Renaissance period.

The investigation here gives analyses of a typical body (paste) area mapped at x400 (*ca.* 320x220µm area) with mineral inclusions, typically ranging between 15-70µm across or in length, set in a fine network of interconnecting relict clay/glass phases (Figure 3). The microstructure, observed by backscattered electron imaging shows the mineral distribution, and the EDX-maps highlight the elemental concentration of the minerals (Figure 4a and b) and the quantitative analyses of these minerals provides their likely identification from the major element proportions present and the consistency with which these analyses occur on different analysed grains within an area (Figure 5). Combining the results of BSE compositional imaging, element distribution maps and quantitative analyses, the maiolica sample body consisted predominantly of quartz, feldspars, chlorite, mica and other less abundant mineral inclusions, such as pyroxene (Figures 3 and 5). FE-SEM high resolution imaging at increasing magnification of the body (paste) of the maiolica can be seen in Figure 3 (x400 – x10000) displaying increasing detail of the interstitial fired clay particles, the range of mineral grains, and the interaction zones and glassy phases of the matrix fusing the particles together.

Elemental mapping

On the basis of the compositional maps for Si, Al, Na, K, Ca, Mg, and Fe (and O) (Figure 4a) together with the quantitative analyses of selected mineral inclusions within that area (Figure 5, Table 1), the rounded quartz grains, were readily identified by the Si map, in which they are visible as white on red areas and also by being absent from all the other maps (dark areas). Rounded potassium feldspar grains were identified from the Si, Al and K maps (Figure 4a) in which they are visible as colour concentrations co-existing (overlapping) the same mineral areas. Similarly, the much rarer, rounded sodium feldspar grains are visible, in particular) as one larger grain in the Na, Si, Al maps. In a different map area (Figure 4b), there are a number of surviving longer acicular particles having the layered morphology characteristic

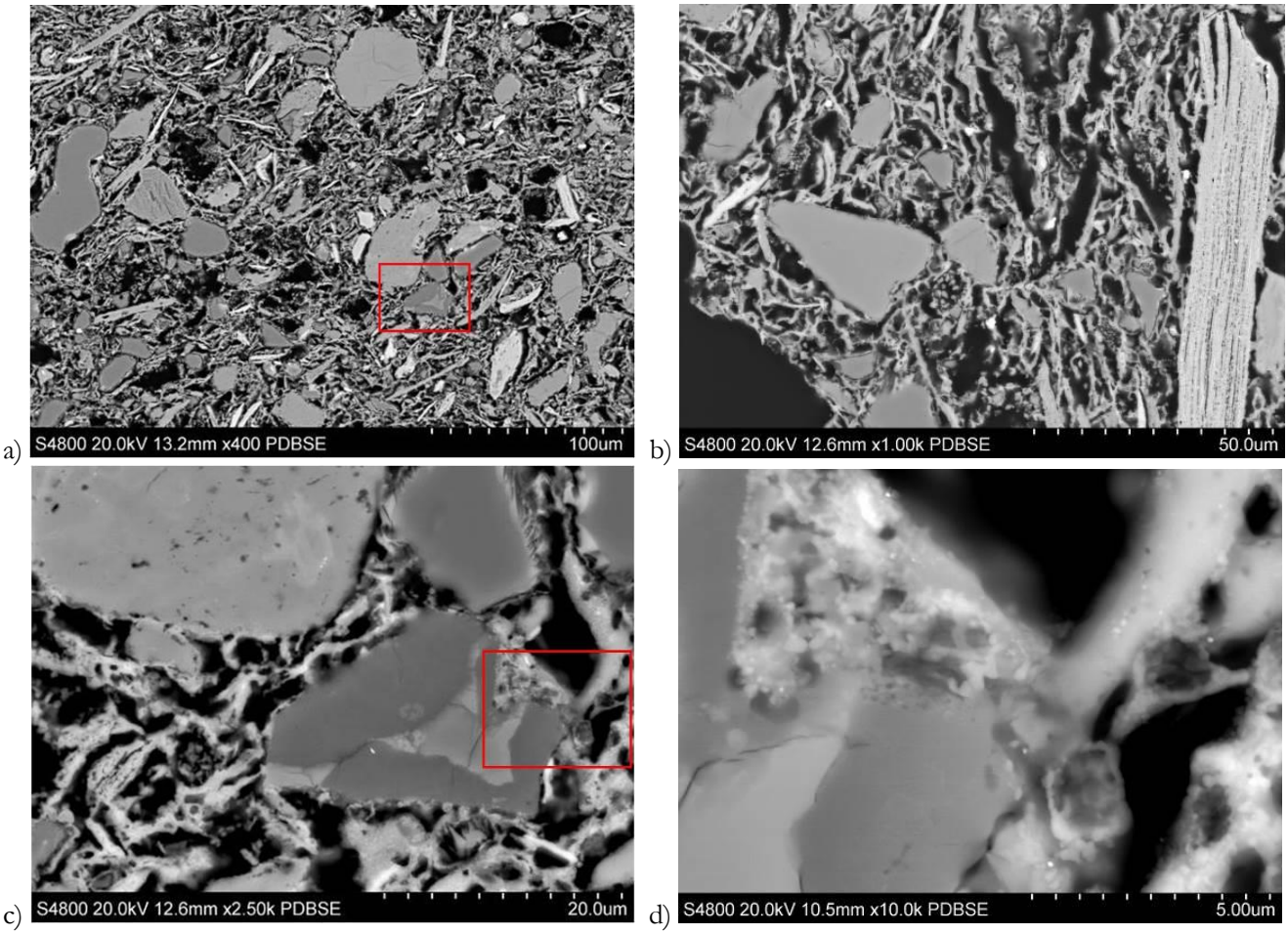

Figure 3. Maiolica sample TW01 paste at increasing magnifications a) x400, b) x1000, c) x2500, d) x10000, showing the mineral grains, layered mica (b), and the glassy filaments binding minerals in the fired clay matrix (d).

of mica, which is confirmed by the correlation between Mg, K and Fe (Figure 3b and map Figures 4a and 4b). In addition, within the area of the polished section illustrated in Figure 5, there is a single, slightly triangular, pyroxene (clino-enstatite) grain which is visible as the large white on red grain in the Mg map, and as a corresponding pale green-blue grain in the Si map (Figure 4a and Figure 5 - Table 1 spectrum 3). Table 1 comprises quantitative analyses of the bulk composition and a number of the more prominent and smaller mineral grains in the ceramic body mapped area, and Figure 6 illustrates typical spectra from Table 1 representing specific minerals present by showing their characteristic elemental signatures.

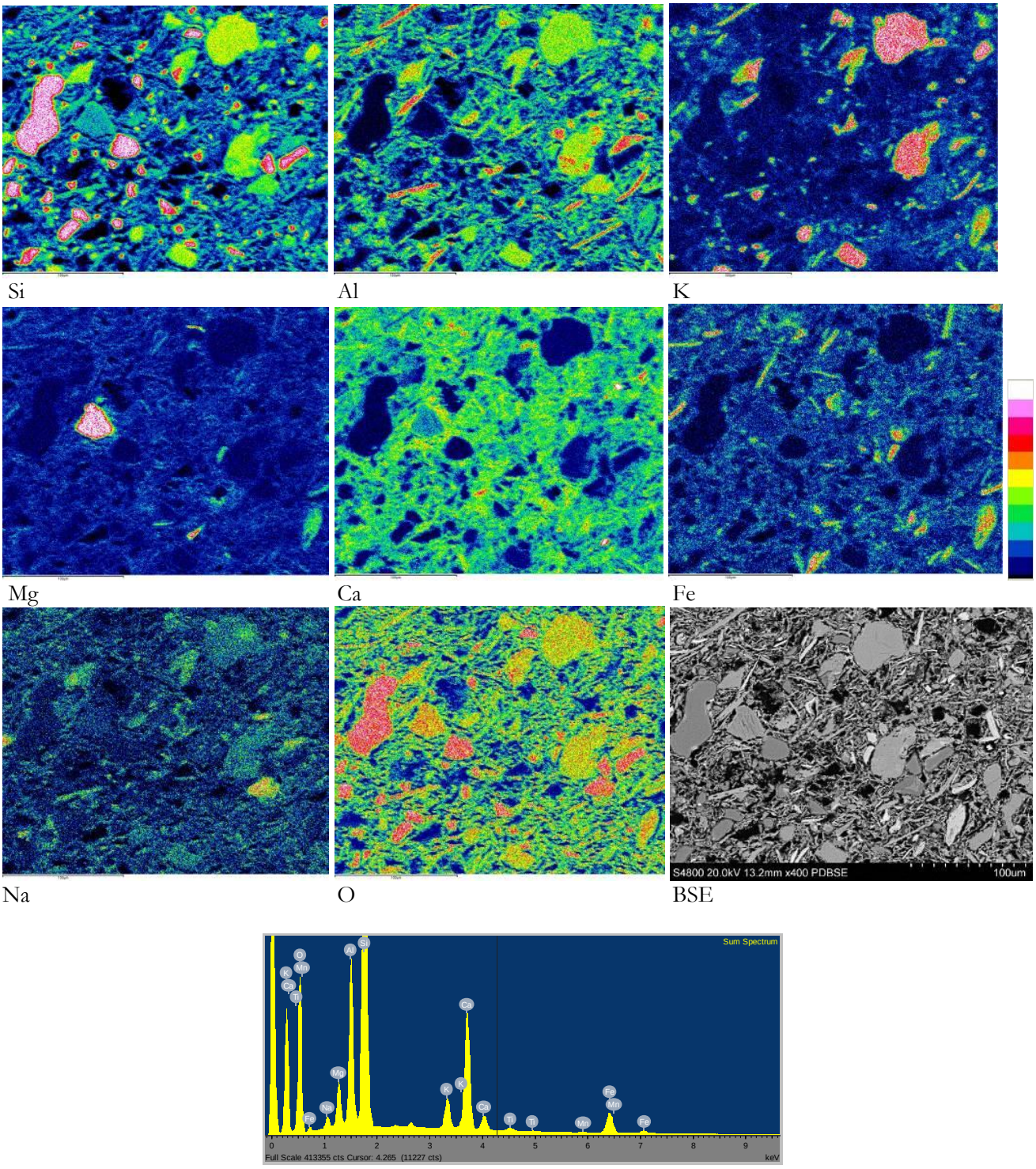

Figure 4a. EDX element maps (x400, width of image 300µm) showing relative element concentrations between minerals and paste. Note the uniformly distributed calcareous paste and overall oxide (oxygen) concentrations, whereas few calcitic mineral grains appear in the paste map. Bottom: map area sum spectrum of the paste, with high calcium peak denoting the overall distribution in the paste area.

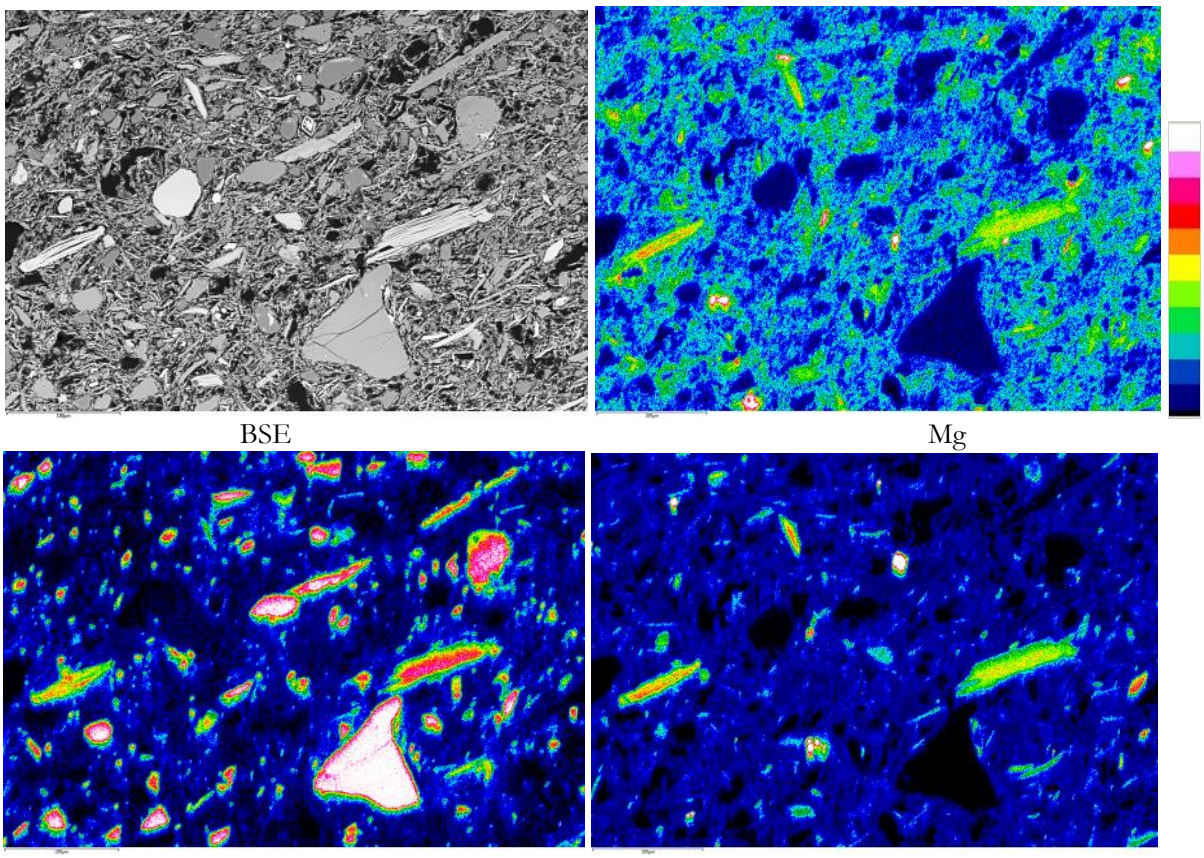

Figure 4b. TW01: element maps (x240) of a different area of the maiolica paste, showing correlation of Mg with K and Fe in the laminated shape characteristic of biotite mica.

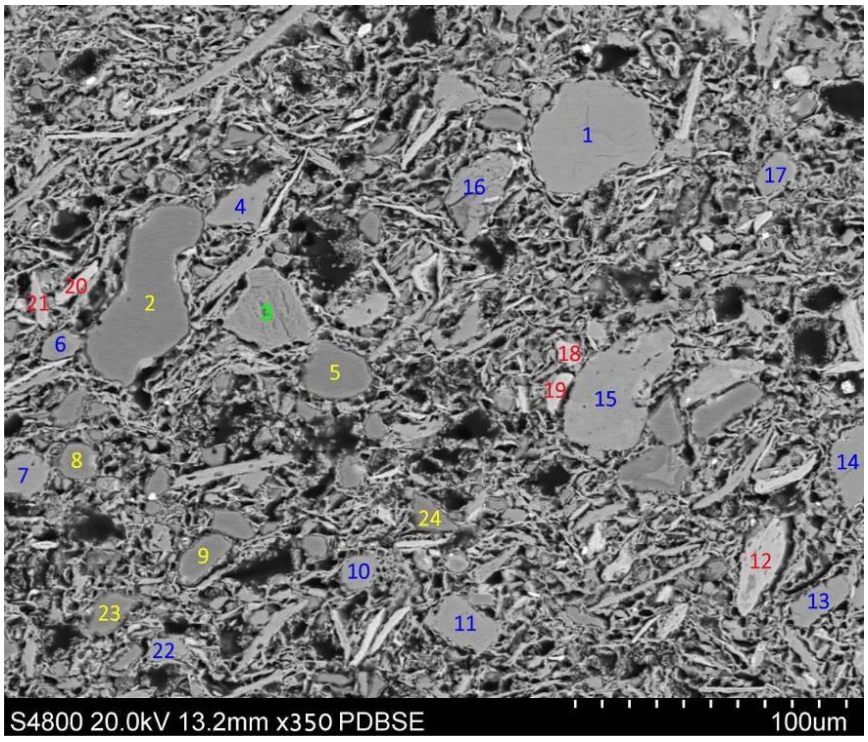

Figure 5. Sample TW01: BSE image of the mapped area with individul spot analyses of the minerals. Note the grey level differences in the BSE image between different mineral types. There are two principal mineral groups and two less common minerals in the paste; legend: quartz Si; feldspar: K, Si, Al; chlorite group: Mg, Si, Fe, Al, K, Ca: Pyroxine/Clino- enstatite Mg, Si, Ca grain (see also Table 5 below).

Table 1: TW01, paste area map: typical analysed minerals with their spectra, see Figure 5.

Mineral Spectra	wt% oxides								
	Na	Mg	Al	Si	K	Ca	Ti	Mn	Fe
Spectrum 2	0.0	0.0	0.0	100.0	0.0	0.0	0.0	0.0	0.1
Spectrum 3	0.2	41.9	1.6	46.3	0.3	7.4	0.1	0.1	2.6
Spectrum 15	1.8	0.0	19.2	64.0	13.1	0.9	0.0	0.0	0.3
Spectrum 20	0.5	9.5	20.3	33.4	5.5	7.6	0.2	0.3	20.4
Mapped area	1.3	4.4	15.4	56.7	2.8	13.3	0.6	0.13	5.4

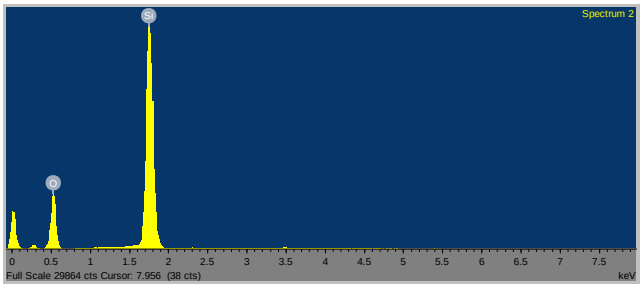

Spectrum 2: Quartz; Si, O

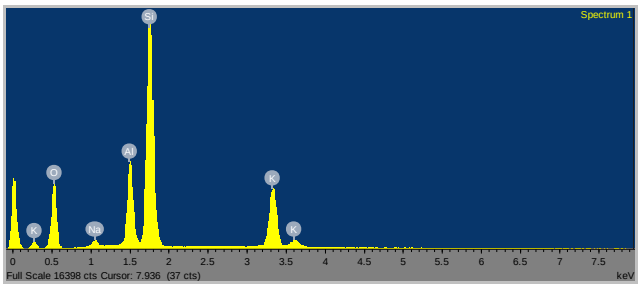

Spectrum 15: Feldspar; Si, Al, K, O

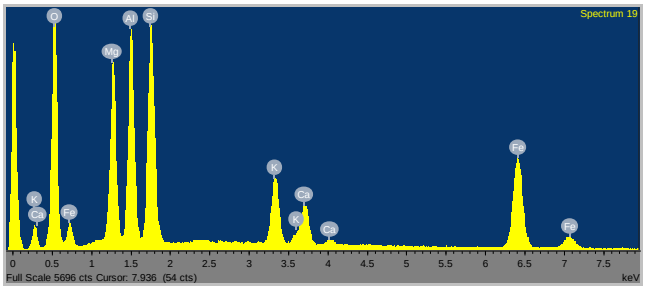

Spectrum 20: Chlorite group
Si, Al, Mg, Fe, O (plus lower K, Ca)

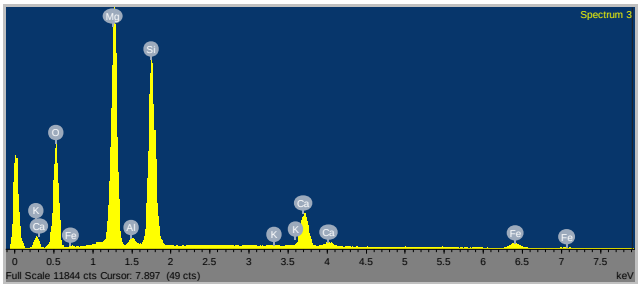

Spectrum 3: Pyroxine/clino-enstatite Mg, Si, O,
single grain (plus small Ca, Fe, Al peaks)

Figure 6. Selected spectra from Figure 5 in Table 1.

Apart from a very few, small lime-rich particles (<5µm across), the lime (CaO) content of the body is homogeneously distributed in the paste within which the other mineral inclusions are embedded and fused together with glassy phases and filaments. Overall, the maps show the interconnecting network consisting of calcium aluminium silicates that have incorporated iron oxide, together with limited amounts of a glass phase, which is associated with presence of soda (Figure 3d). The presence of the iron oxide in the silicates resulted in the characteristic buff colour of calcareous clay bodies, rather than the red colour that would have resulted if the iron oxide had survived as haematite.

Glaze

One of the most striking things about the maiolica plate is the intense deep blue colour of the glaze (Figure 1, which is dramatically seen in the polished cross section in Figure 2). The blue glaze applied to the sherd is *ca.* 600 µm thick (at the point of the examination) but is seen as two distinct layers, an inner opaque glaze (*ca.* 420 µm thick) corresponding to the *coperta* layer described by Piccolpasso (*ca.* 1557) of a lighter blue colour, and an outer transparent deeper blue glaze (*ca.* 180 µm thick) (Figure 2)[7]. The two optical blue layers are associated with two distinct glaze layers and glazing events, and are due to differences in the chemical and mineralogical compositions from the manufacturing processes. It is at this point that the power of high-resolution FE-SEM-EDX imaging, analysis and X-ray mapping can be applied to discover their microstructure and composition, and hence the materials used in their formation.

The first noticeable impression of the SEM BSE image (Figure 2d) is the complexity and variety of the mineral components within both transparent and opaque glaze layers. The most noticeable difference being that the region of the optically transparent glaze has less large and mineralised inclusions

[7] The two-colour layer variation was also noted by Tite (2009).

compared with the underlying optically opaque glaze. Understanding the microstructural complexity was approached from two chemical analytical directions: X-ray mapping of the entire field of view at very high pixel density (4100x2900 pixels) to give the overall chemical viewpoint and distribution of minerals and phases, followed by EDX analysis of key regions, minerals and phases. The combination of the two would provide identification of the minerals added, the glaze matrix composition and the glaze colourant and hence the processes of manufacture.

Analysis of the glaze layers

General area analyses of the upper and lower glaze layers incorporate all the minerals in the layers as well as the glassy matrix. Both glaze layers are leaded with low soda and the presence of cobalt as the blue colourant and tin oxide as the opacifier in the lower opaque blue glaze (Figure 7, Table 2).

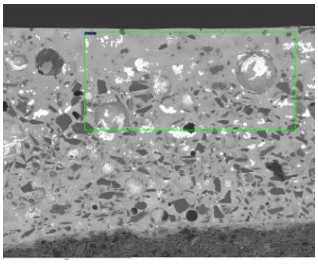

Upper glaze area, Sp1

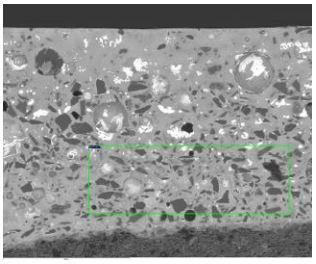

Lower glaze area, Sp2

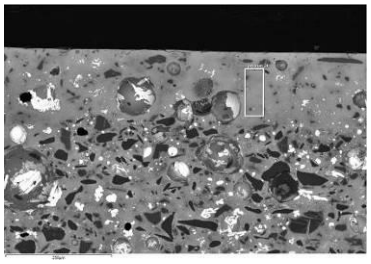

Spectrum 24 area in upper glaze.

Spectrum wt% oxides	Na	Mg	Al	Si	K	Ca	Ti	Mn	Fe	Co	Ni	As	Sn	Pb
Spectrum 1 upper glaze	1.9	0.5	5.0	61.6	6.1	1.5	0.1	0.0	2.3	2.7	1.4	3.1	2.3	11.4
Spectrum 2 lower glaze	1.5	0.4	5.2	66.9	5.6	1.4	0.1	0.0	0.8	0.8	0.3	1.2	3.9	11.9
Spectrum 24 upper glaze free of mineral inclusions	2.1	0.5	4.7	58.9	6.7	0.9	0.1	0.0	3.4	2.4	0.6	1.3	0.3	13.5

Figure 7 & Table 2. General area analyses of the upper and lower glazes (spectra 1 and 2). Note how the cobalt, nickel and iron values in the different areas correspond well to their relative concentrations in the maps (Figure 15 below). Note also Spectrum 1 clips the lower glaze so that more tin is incorporated - see Sn map. Whereas an area of the upper transparent glaze above the tin oxide opacified lower glaze has much reduced tin, spectrum 24 (see Sn map Figure 12).

EDX high resolution maps of the complex glaze of the polished maiolica sample

EDX maps of the glaze show clearly defined mineral grains with elemental associations combined for specific minerals, and diffusion zones and concentrations within the glaze (Figures 8, 9, 10, 11, 12, 15, 18). Element lines for maps were chosen to avoid overlapped peaks and results checked by EDX analyses, for example Pb and As, Sn and Ca as these are important fingerprint elements in the glaze, and also Co, Ni and Fe as these are associated with the blue colourant and its associated remnant minerals. In addition, potential overlapped X-ray lines such as As 'L' and Mg 'K' can be further interogated by the feature 'Truemap' within the Oxford Instruments analyser which does complex peak subtractions at overlap regions.

Quartz and felsdspars

Quartz grains are clearly identified by the white-coloured mineral concentrations in the Si map distributed mainly within the lower glaze areas (Figure 8). The positions of these angular grains also show as corresponding black areas on other maps (e.g. Figure 9, K map). Potassium feldspar grains are identified by the association of Al and K concentrations in the same mineral grains throughout both the outer transparent and inner glaze layers (Figure 9), and are slightly angular and are present in slightly smaller numbers.

Note that the silica contents of the feldspars are similar to those of the dissolved silica in the glaze itself (i.e. some 60 wt% SiO_2). These feldspar grains cannot be seen on the Si map, even as outline shapes, as they merge seamlessly into one uniform silicon concentration distribution (Figure 8). It is therefore important to map each of the main elements and compare all of the maps for correlation within mineral grains.

The Na map shows low soda, characteristic of lead-alkali glazes, throughout the glaze layers, but occasional sodium feldspar grains were identified as the cluster of three white grains in the lower glaze, one larger and two smaller adjacent grains (Figures 10 and detail Figure 11).

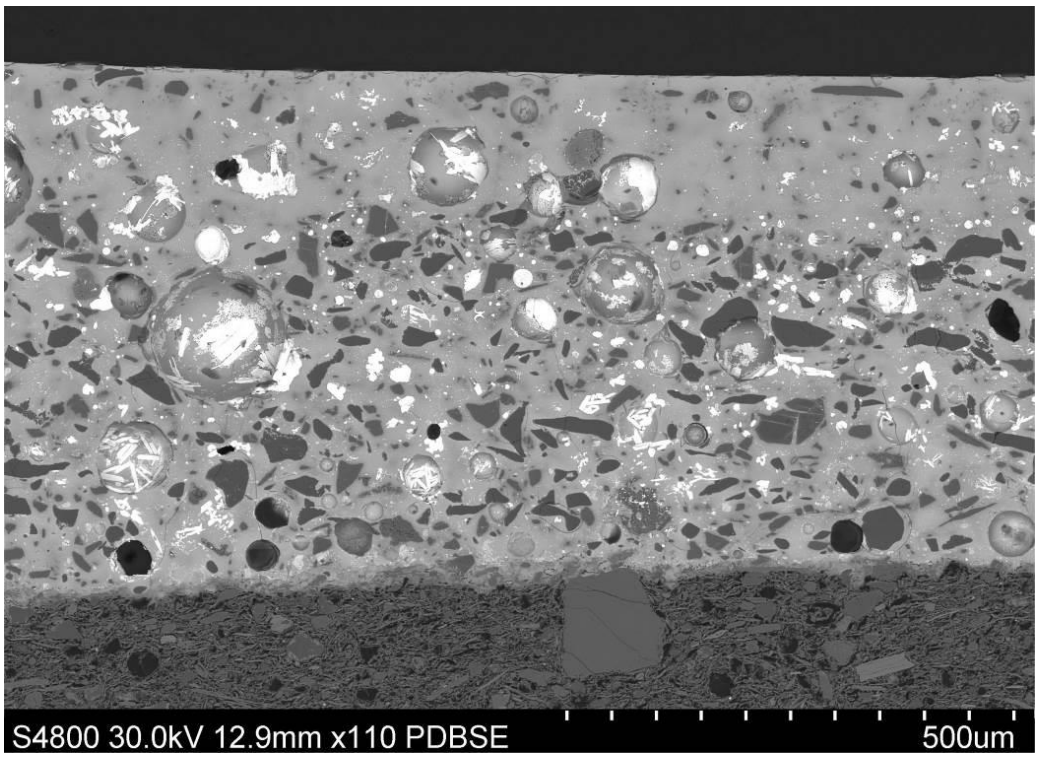

SEM BSE image

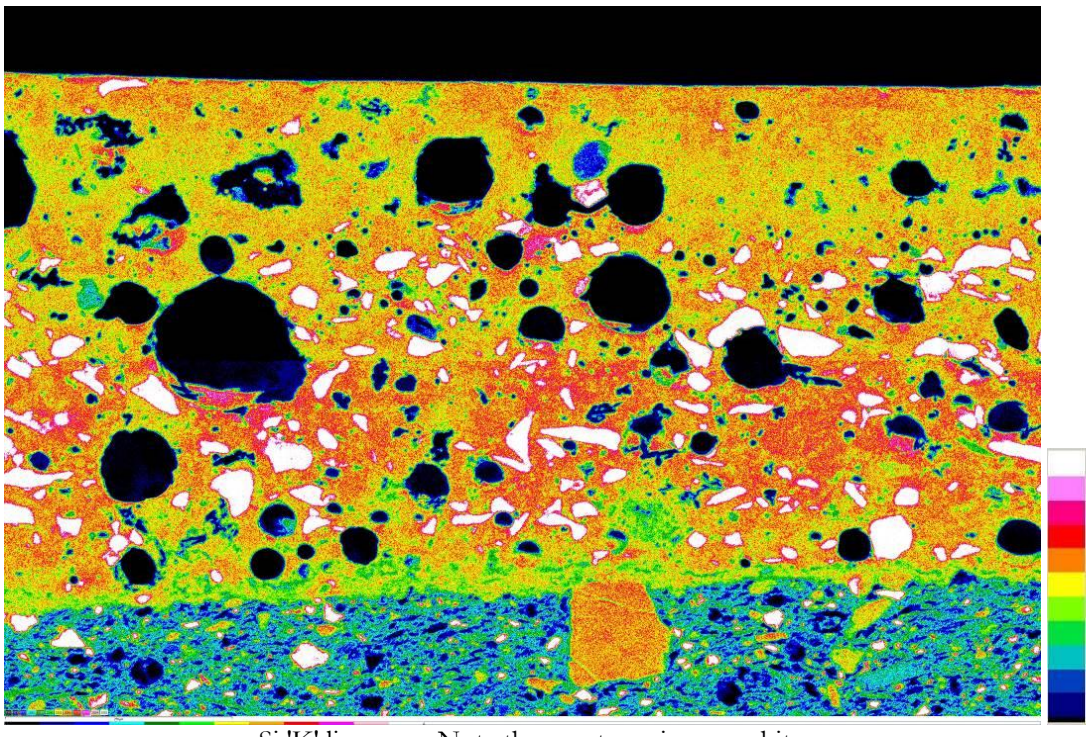

Si 'K' line map. Note the quartz grains are white.

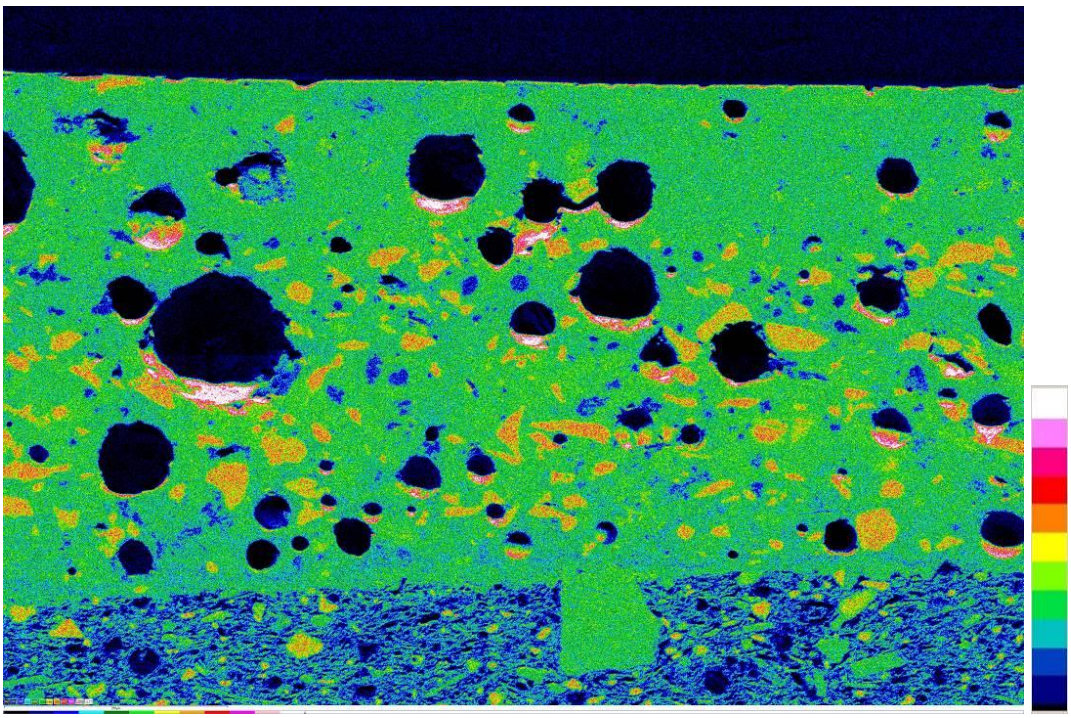

O 'K' line map. Note the quartz grains are orange.

Figure 8. Top, SEM-BSE image of the region examined in detail by SEM-EDX mapping and analysis c. 1x0.8mm area at x110. Note the gas porosity in the glaze shows as round black holes in the maps due to the X-ray detector having low-angle geometry, but the BSE image shows crystalline features in these pores because the electron detector is directly above the area.

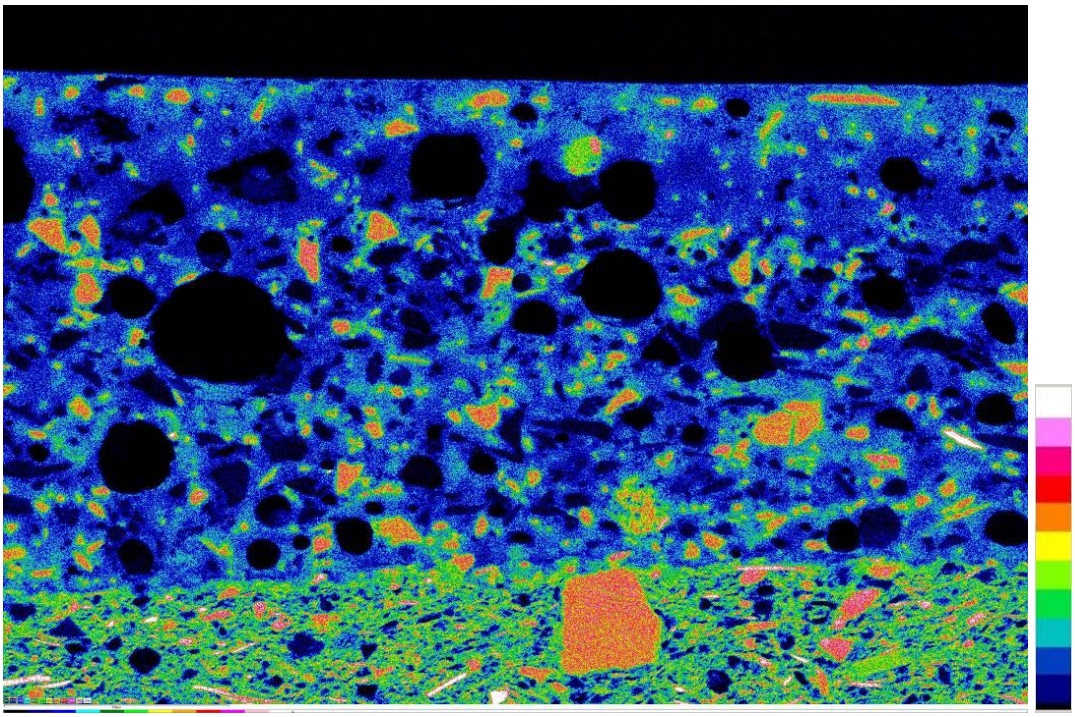

Al 'K' line map. Feldspar grains are orange.

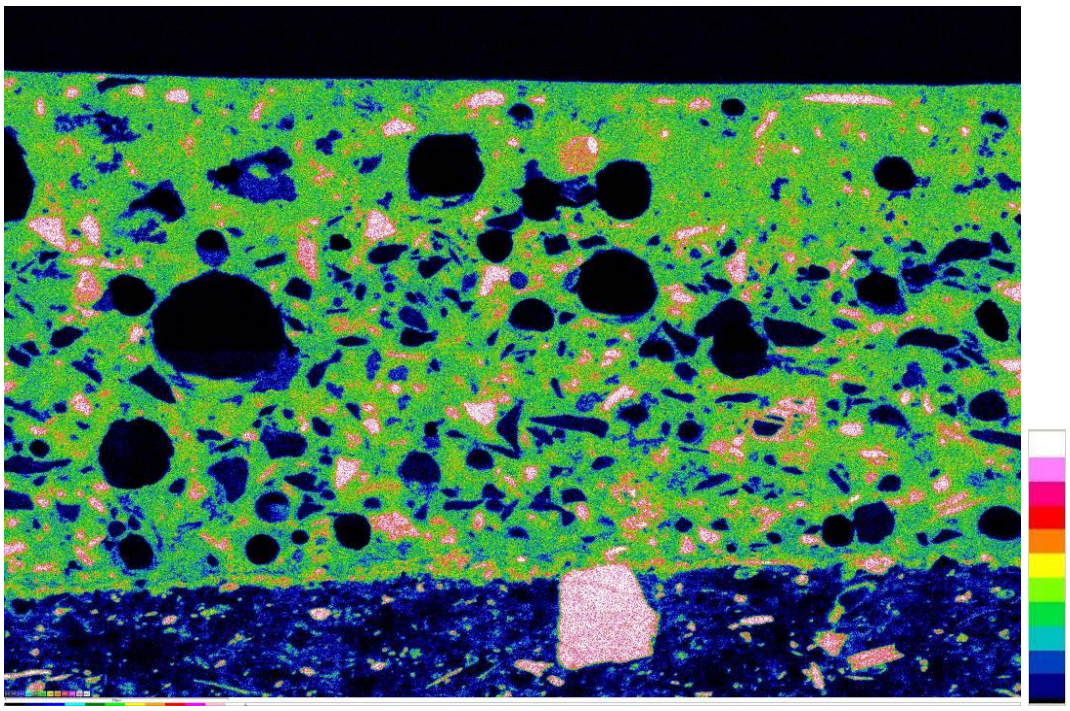

K 'K' line map

Figure 9. Feldspar grains (Al, K silicates): association of concentrations in the Al and K maps. They are throughout the two glaze layers and within the ceramic paste.

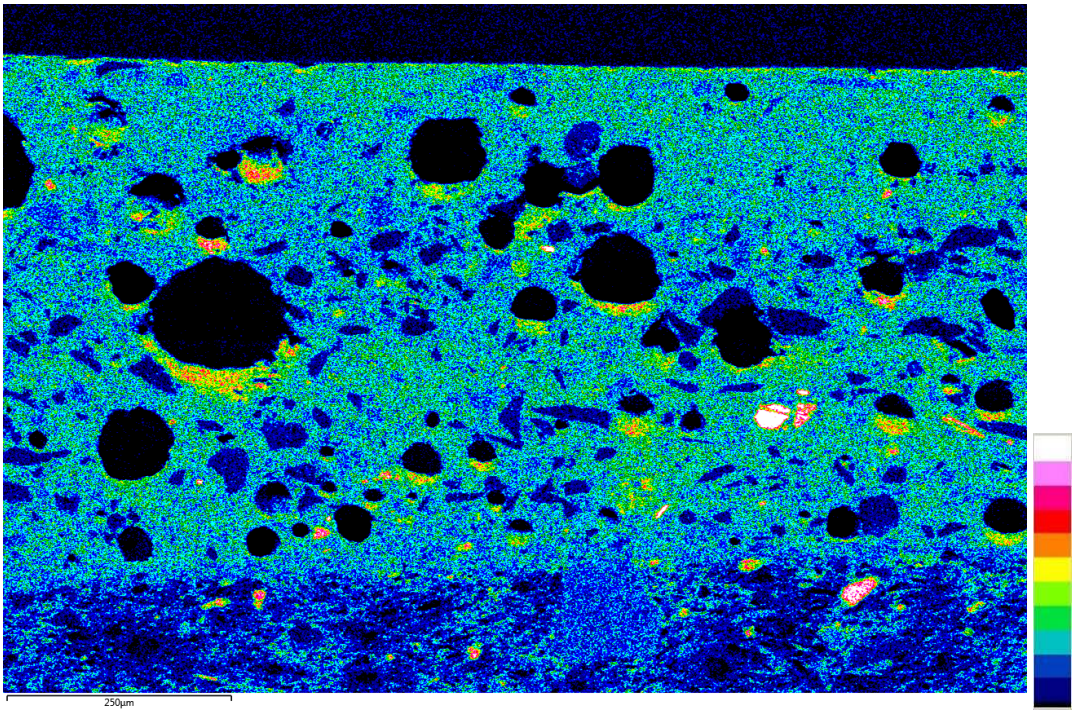

Na 'K' line map

Figure 10. TW01, Na map: generally low soda content of the glaze (c 2.1% Table 2 spectrum 24) and ceramic paste. Note the occasional Na feldspar grains (white, and see detail in Figure 11).

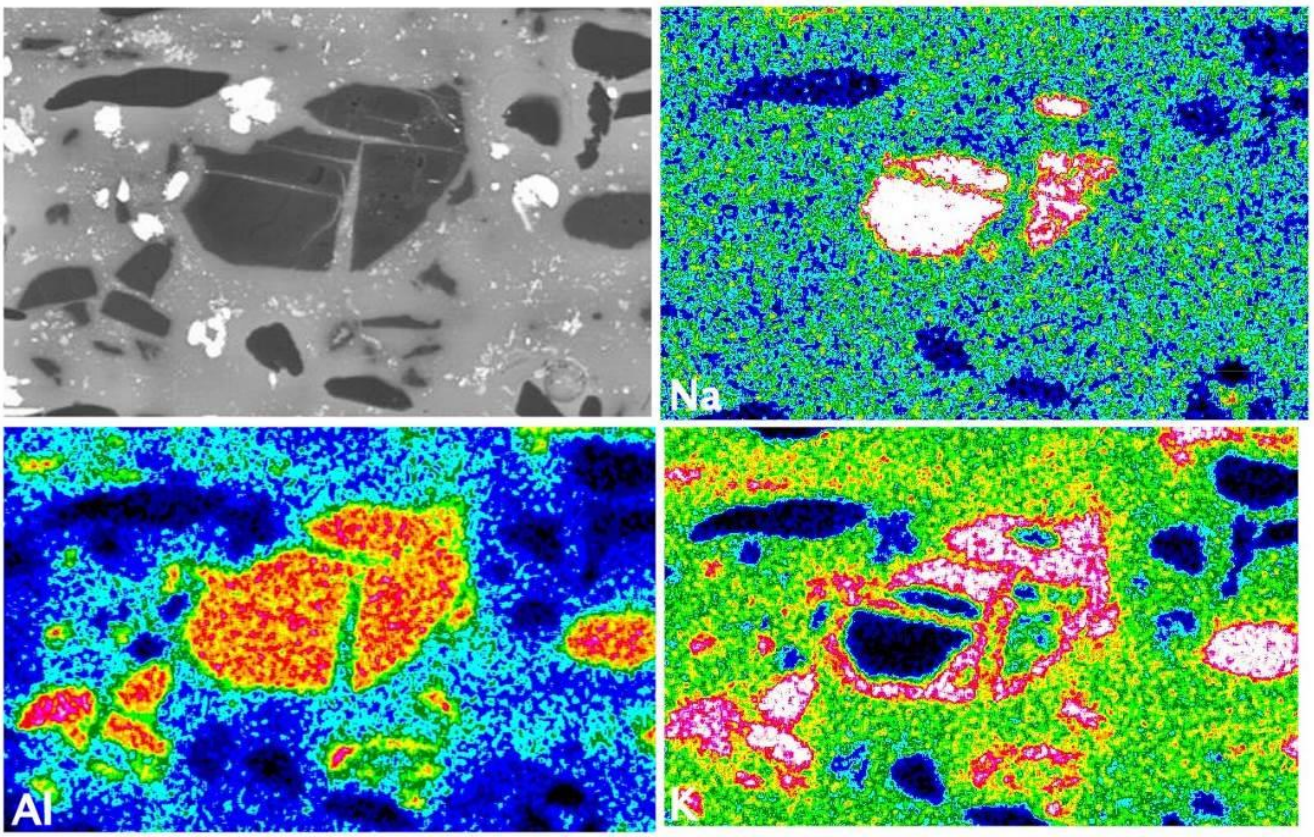

Figure 11. BSE image and selected map area detail of the complex Na/K/Al feldspar mineral grains extracted directly from the full area high resolution maps (Figures 9 and 10). Width of each map 165μm.

By extracting detail maps from the original high-resolution map, it becomes clear that the feldspar mineral is a fractured grain having a composite Na/K two-phase morphology (Figure 11). This is a good illustration of the way an original 4100x2900 pixel high-resolution map retains all the chemical and morphological information in a single map image and allows digital zoom interrogation retaining a good resolution image. It also illustrates the point to be aware that different chemical phases within a mineral grain can have similar BSE grey level contrast images by having similar mean atomic numbers (Figure 11), and even similar relative levels of a particular element; in this case Al which shows a uniform concentration in the large central grains (red/yellow), and on its own masks the complex mineralogy which is revealed by the Na and K element concentrations seen in different regions within the same grain.

Tin oxide opacifier, inner glaze

The Sn map (Figure 12) shows the inner opaque glaze layer (*ca.* 420 μm in thickness) has a fairly uniform distribution of mainly fine tin oxide particles, present as individual small acicular particles about 1-2 μm long. These are absent in the outer glaze layer. In addition, tin oxide is sometimes present as clumps up to *c.* 30 μm across (Figure 13 and image in Table 3), whereas others are much smaller and seen at 20,000x magnification, as individual acicular sub-micron crystals, *ca.* 0.44x0.1 microns in size, some of which appear to show some microscopic crystal orientation in the glass (Figure 14a-c). Molera *et al.* (1999) also show medieval tin glaze has a particle size of tin oxide of around several hundred nanometers, which corresponds to the range of wavelength of visible light. They also noted that in some cases, the tin oxide is presented not only as small crystals but also as aggregates of particles. These factors – the high refractive index, the low solubility in glazes and the particle size make tin oxide an excellent opacifier.

This inner glaze also has a distribution of quartz particles up to about 80 μm across, and fewer feldspar particles up to about 50 μm across which result from the addition of sand to the fritted glazing mixture (Figures 8 and 9, Si, Al, K maps, and also analysed minerals - quartz spectra 13-15 & 17 and feldspar spectrum 16, Figure 19 and Table 6b).

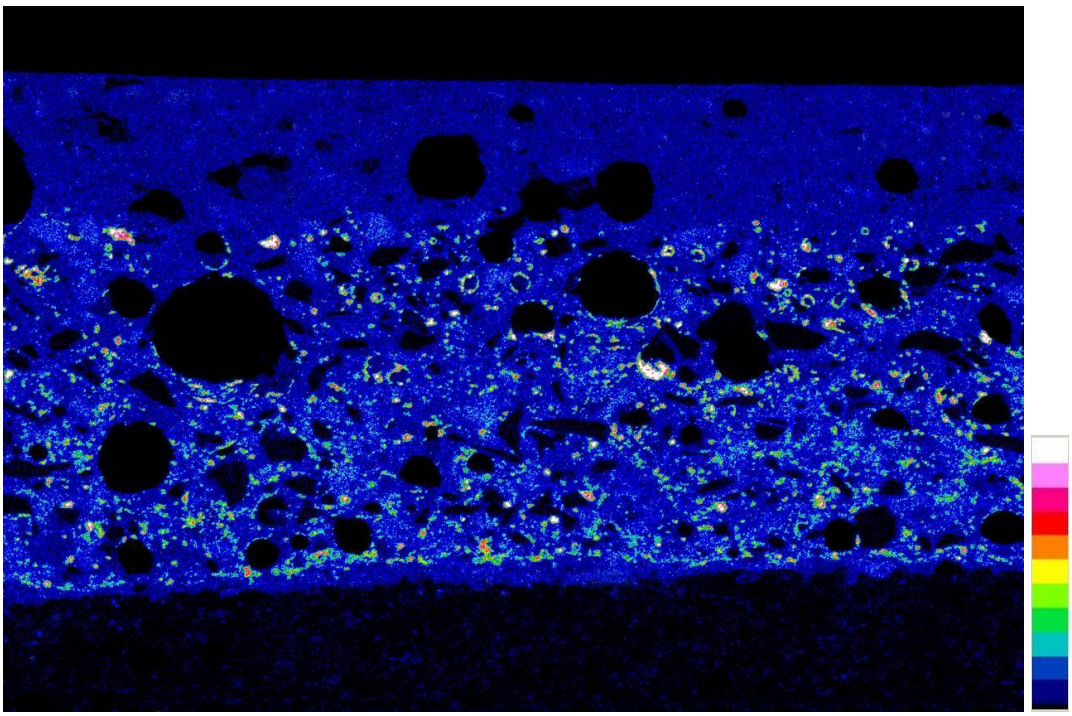

Sn 'L' line map

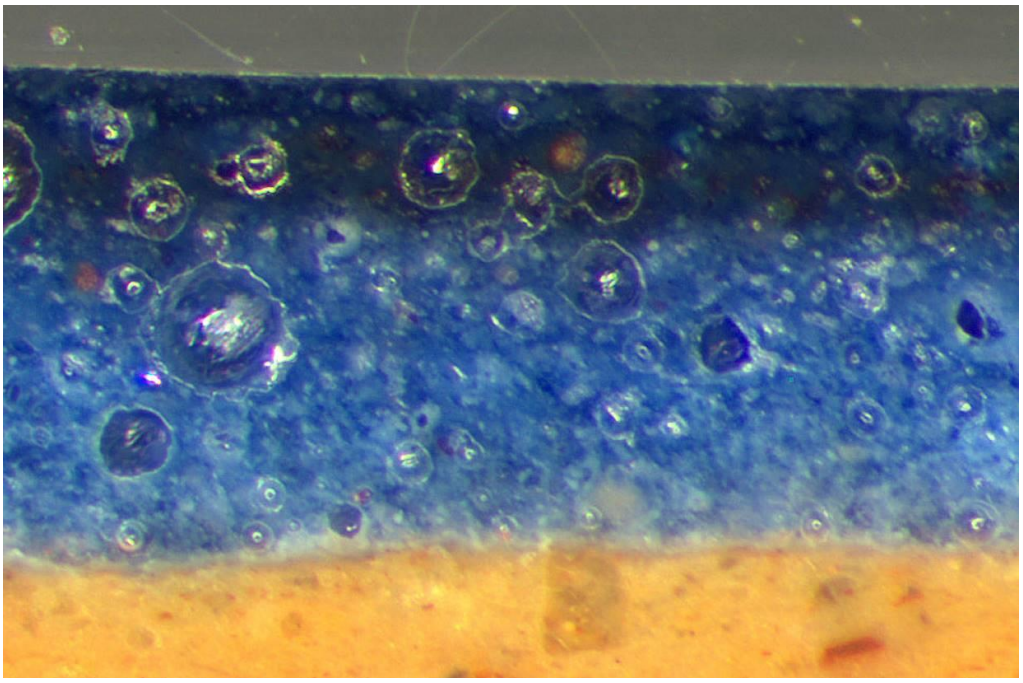

Figure 12. TW01: Sn map (top image) showing tin (oxide) concentrated in the inner glaze as bright particulates, which corresponds to the opacified lighter blue lower glaze in the optical image (also Figure 2). There are no tin (oxide) particles in the upper transparent glaze.

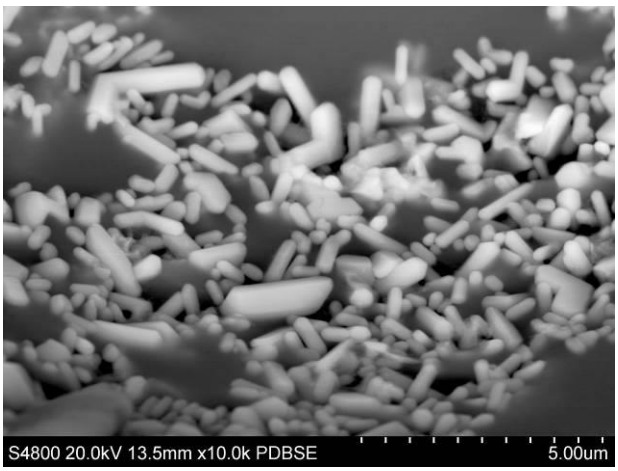

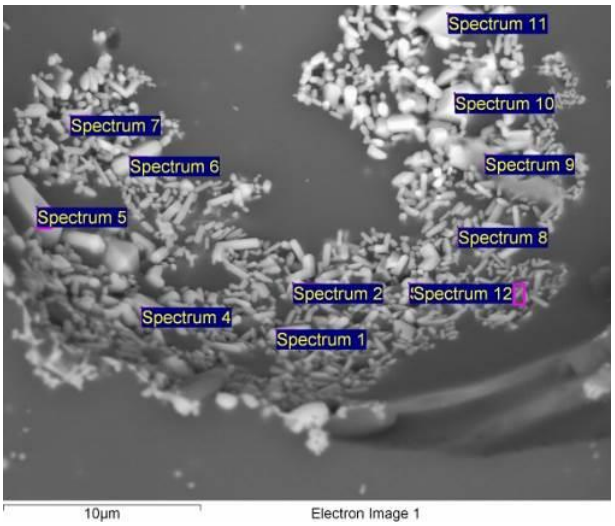

Figure 13. Upper: Tin oxide crystals precipitated in the glaze at the surface of a gas bubble (x10,000). Lower: point analyses on crystals. See Table 3 below.

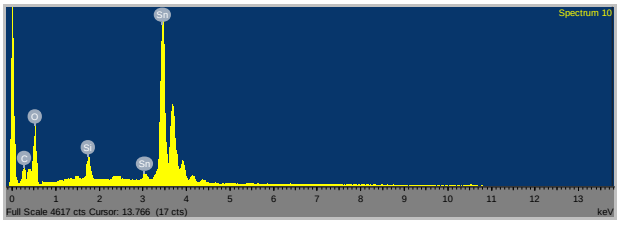

Spectrum wt% oxides	Sn	Si	Pb
Spectrum 4	88.5	7.5	1.2
Spectrum 10	90.0	6.9	1.3

Table 3. Spectrum 10: typical spectrum of a larger tin oxide crystals seen in the surface of a gas bubble. Key elements Sn, Si, Pb in their relative concentration selected from analyses (spectra 4 and 10). Note, the Si and Pb contributions are from beam penetration through the tiny crystals of tin oxide and scatter from the glass matrix below. The spectra with highest tin show less scatter (i.e. the largest crystals Spectrum 10, compared with 4).

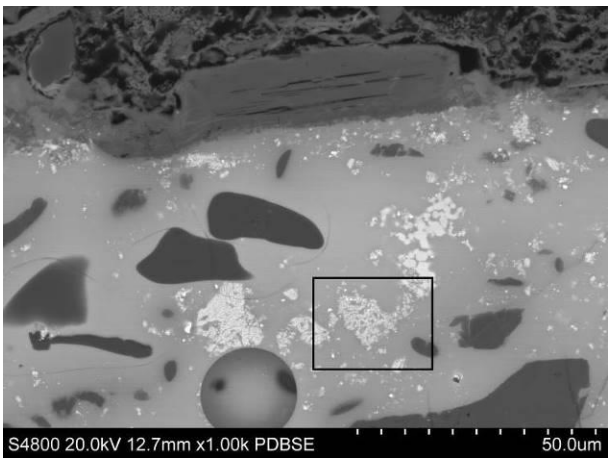

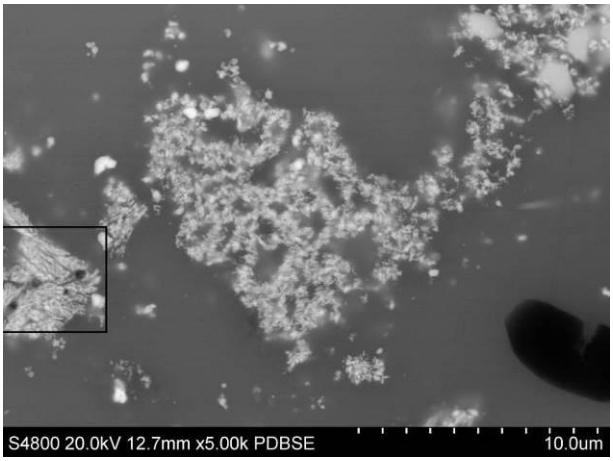

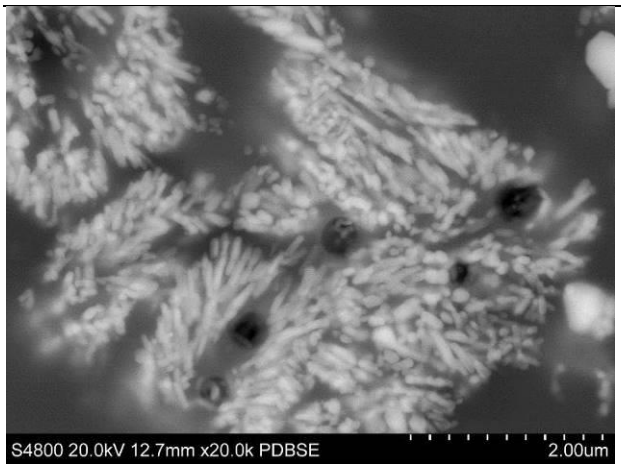

Figure 14. TW01, tin-rich particles at x1000, x5,000 and x20,000 magnification. The white-coloured tin oxide particles that form in the blue glaze are the opacifiers to make it appear opaque and intensely blue. The individual acicular crystals are ca. 0.45x0.1 microns in size.

Outer glaze

In contrast, the outer transparent glaze layer (*ca.* 250 µm in thickness), which corresponds to the *coperta* layer described by Piccolpasso, was more or less clear of quartz and tin oxide particles (Figures 8 and 12) but contains feldspar grains (Figure 10, maps for K and Al). This two-layer glaze type contrasts with a

single opaque glaze layer, which was also widely used in the production of Italian maiolica ceramics during the Renaissance period. Further, both glaze layers applied to sherd TW01 were of the lead-alkali type (Tite *et al.* 1998) containing around 13.5 wt% PbO and some 8.8 wt% total alkali (Na_2O + K_2O) (Table 2 spectrum 24). The silica content dissolved in the glass phase of the outer glaze was slightly lower than that of the inner glaze, and without quartz gains (see map Figure 8 for relative Si concentrations). This would help to reduce the melting point of the outer glaze that was added in a second process.

In addition to compositional glaze maps for Si, Al, Na, K, Ca and Fe, equivalent to those for the body of the sherd, additional elements present in the glaze layers were also obtained: Sn, Co, Ni, Pb, As (Figures 12, 15, 18), together with quantitative analyses for selected areas and phases (Tables 2, 3, 4, 5, 6). The Sn map provided a clear demarcation between the opaque inner glaze containing abundant tin oxide particles (map Figure 12) which are visible as small bright precipitated areas in the optical micrograph (Figure 2)**,** but tin oxide particles are absent from the transparent outer glaze.

Cobalt colourant and remnant minerals

The striking blue colour of the glaze is seen in the sample cross section, Figure 2. Cobalt is dissolved throughout both glazes and is the blue colourant for this glass. The element maps of this section clearly define the association of cobalt (Co), nickel (Ni), and iron (Fe) in a band of remnant mineral particles above the lower glaze layer (Figure 15).

These remnant particles of the cobalt pigment are clearly visible as concentrated bright mineral areas in a distinct broad band at the interface between the two glaze layers on the Co map. It appears that the cobalt-rich mineral grains were applied to the surface of the inner opaque glaze before the application and firing of the transparent outer glaze. Cobalt had diffused during firing throughout the thickness of the outer transparent glaze (*ca.* 2.4 wt% bulk CoO), the colour of which is dark blue; the cobalt also diffused into the opaque inner glaze (*ca.* 0.8 wt% bulk CoO, Table 2), the colour of which is a paler blue. The colour difference is partly due to the lower concentration in cobalt in the inner glaze but also due to the presence of the white coloured tin oxide opacifier crystals already in the underlying first glaze layer. Note that the cobalt dissolved in the glass adjacent to the mineral complex (Figure 16 spectrum 5) is higher than the overall glaze levels due to the dissolution from the nearby cobalt-containing mineral grains. The Ni map matches almost exactly that of the cobalt map, indicating that nickel was introduced with the cobalt pigment (Figure 15), while Figure 16 and associated Table 5 show some primary cobalt/nickel silicate mineral grains (highlighted orange spectra 3, 4, 7, 8).

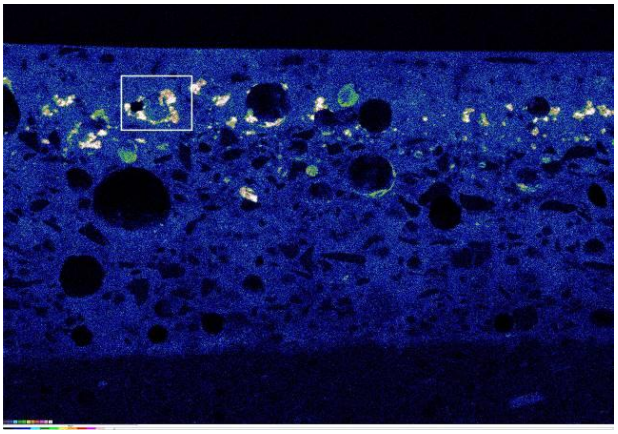

Co 'K' line map

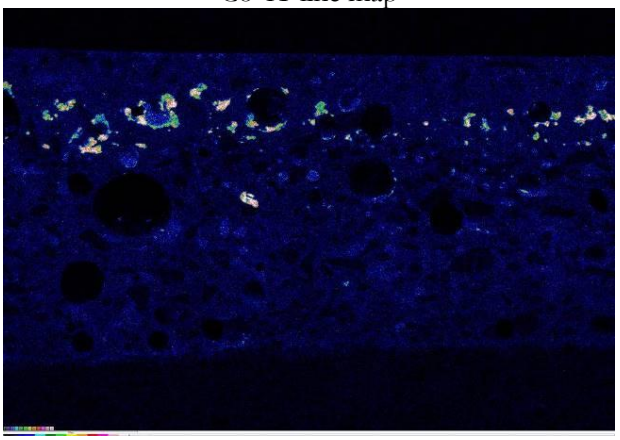

Ni 'K' line map

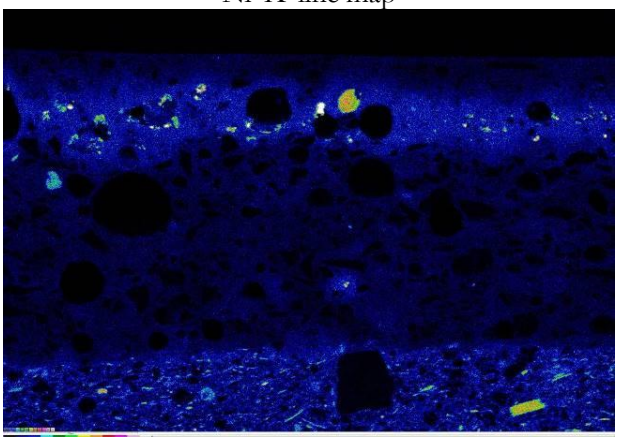

Fe 'K' line map

Figure 15. TW01: cobalt and nickel are in association with each other in remnant minerals containing the cobalt for the blue glaze colouring. Note the Cobalt has diffused throughout the two glaze layers and iron predominantly only within the band in the outer transparent glaze (and is also seen as a constituent of the pottery paste). Square in Co map is the detail area in Figure 16.

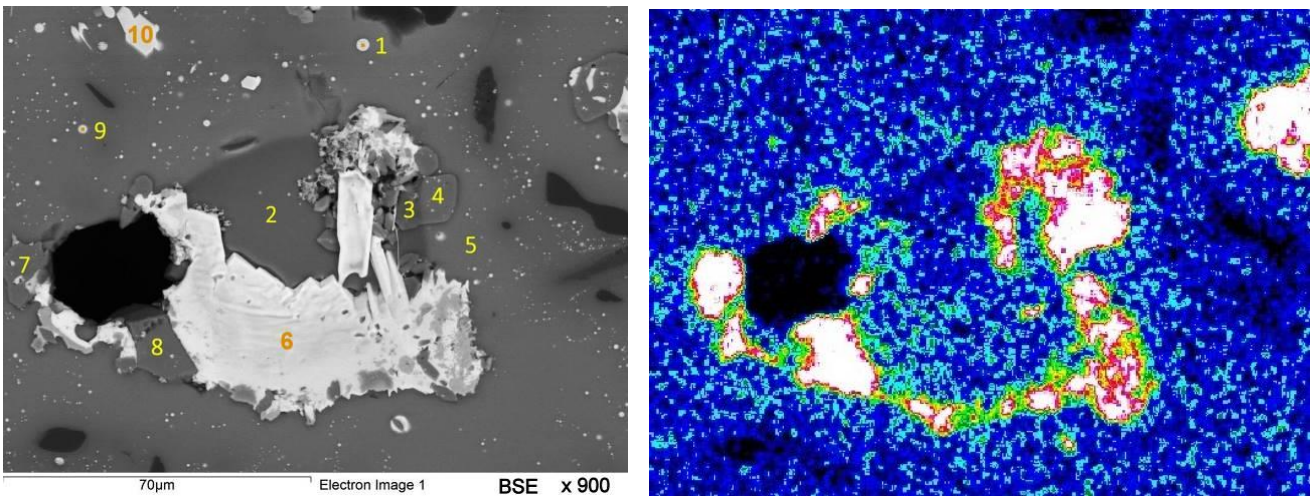

Figure 16. TW01, mineral complex in cobalt-rich area located in the outlined oblong area in the Co map Figure 15 from which the map detail area is taken from this original high resolution map. Note how the Co map clearly shows the individual analysed high-Co/Ni grains, spectra 3, 4, 7, 8 around the large Pb/As mineral grain spectrum 6.

Table 5. TW01, Analysis of complex mineral group in the glaze of Figure 16. Spectra associated with cobalt minerals (main elements - orange and green) and calcium-lead arsenate mineral grains (main elements - blue) (See also Table 6a). Purple is in the glaze area.

Spectrum wt% Oxides	Na	Mg	Al	Si	K	Ca	Ti	Mn	Fe	Co	Ni	As	Sn	Pb	Total
Spectrum 1	2.3	0.4	0.7	15.8	1.7	9.5	0.1	0.2	0.9	5.9	2.4	24.6	0.2	35.3	100.0
Spectrum 2	1.0	0.3	2.3	38.1	6.9	0.9	0.1	0.0	21.4	14.9	2.5	2.7	0.6	8.6	100.0
Spectrum 3	0.1	3.9	0.0	19.4	0.2	0.2	0.0	0.1	0.5	33.4	37.6	3.4	0.2	1.2	100.0
Spectrum 4	0.0	1.2	0.1	27.7	0.0	0.1	0.0	0.0	1.0	30.0	38.0	1.3	0.1	0.7	100.0
Spectrum 5 glaze	1.8	0.4	3.2	62.9	7.0	0.7	0.1	0.0	4.9	3.0	0.5	1.4	0.8	13.4	100.0
Spectrum 6	2.9	0.0	0.1	1.9	0.6	11.9	0.0	0.0	0.4	1.2	1.2	34.9	0.0	45.3	100.0
Spectrum 7	0.1	4.3	0.1	28.7	0.1	0.2	0.0	0.0	1.4	28.6	34.6	0.9	0.4	0.7	100.0
Spectrum 8	0.0	4.5	0.0	30.9	0.1	0.1	0.1	0.0	0.4	28.3	33.2	2.1	0.0	0.4	100.0
Spectrum 9	2.5	0.5	1.1	17.4	2.0	8.3	0.1	0.1	1.1	6.1	2.1	25.4	0.2	33.0	100.0
Spectrum 10	1.1	0.0	0.1	1.7	0.7	20.6	0.0	0.1	0.3	0.7	0.0	29.7	0.8	44.5	100.0

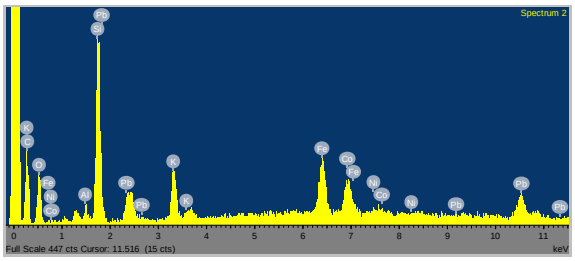

Spectrum 2. Fe, Co, Ni, silicate mineral

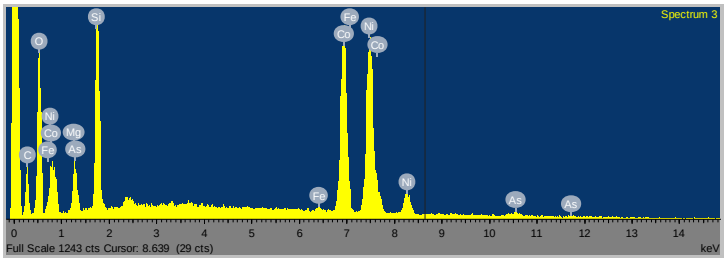

Spectrum 3. Co, Ni, silicate mineral

Iron association with remnant minerals

There is also a general associated matching between the iron map (Figure 15) along the same broad band containing the remnant cobalt/nickel particles in the transparent blue glaze. Some concentrations of iron are found in minerals (brightest regions in Figure 15) that are seen directly associated in aggregates with the cobalt/nickel silicate mineral grains (in Figure 16 and Table 5 spectrum 2). Iron is diffused within this outer glaze from this mineralised band, although not uniformly throughout this glaze layer, as shown in the small area analyses (Figure 17). The iron, which is much less mobile than cobalt, was almost certainly introduced along with the cobalt minerals.

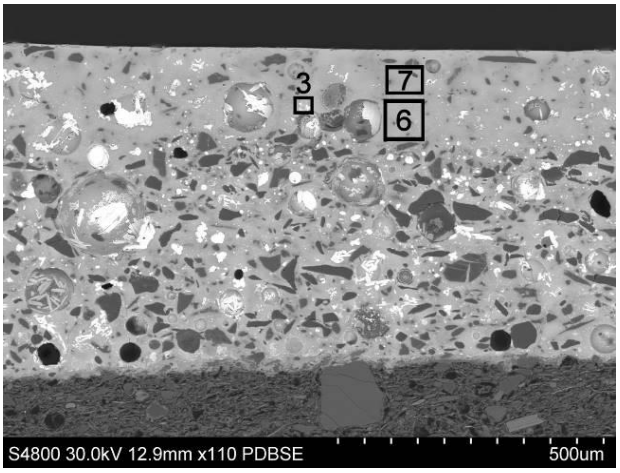

Spectrum	FeO%	CoO%	NiO%
3 mineral	29.4	15.3	9.2
6 glaze	4.5	2.5	0.9
7 glaze	1.6	1.6	0.4

Figure 17. TW01. BSE image of the maiolica glaze and small area analyses; relative Fe, Co, Ni concentrations. Note how the ratio of Co/Ni remains relatively similar in the glaze while the Fe is progressively less concentrated towards the surface away from the broad concentrated particulate mineral band in Figure 15 map.

Calcium-lead arsenate crystals

Since arsenic is only present in those Italian maiolica glazes containing cobalt as the colorant, it is certain that the arsenic must have been introduced with the cobalt pigment. As discussed by Zucchiatti *et al.* (2006) and Tite (2009, 2077) the presence of cobalt with arsenic is due to the fact that zaffre is the source of the cobalt colorant which was obtained by roasting arsenic-rich cobalt ore from Saxony in Germany.

The arsenic map (As 'L') shows that the element appears concentrated in a scatter of complex inclusion areas (up to *ca.* 60 μm across) throughout both glaze layers and perhaps a little more concentrated in the lower opacified glaze layer. Analysis of the glaze between the inclusion areas also shows that during firing, because of its volatility, arsenic is diffused more or less uniformly throughout both the outer transparent and the inner opaque glazes (*ca.* 1.3%, Table 2 spectrum 24).

Looking closely at the distribution of the arsenic, its map concentrations match with areas in both the Pb and Ca maps (Figure 18) which indicates the presence of calcium-lead arsenate particles. These are seen associated with complex minerals found in the general region of the band of high cobalt/nickel/iron minerals. This association is clearly seen in Figure 16 (spectra 6 and 10 in Table 5), with the large As/Pb/Ca arsenate particles which are in direct physical contact with remnants of the original complex of cobalt minerals Figure 16 (spectra 3, 4 ,7, 8).

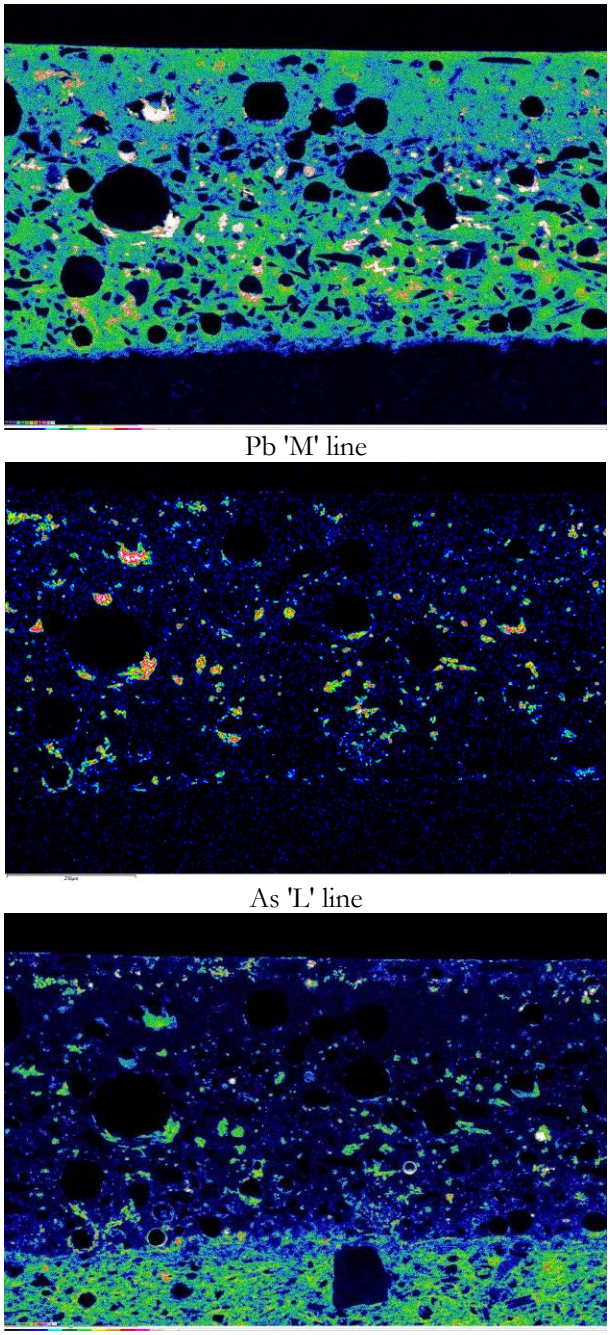

Figure 18. TW01: the glaze layers are both leaded. Note the calcareous ceramic paste and the asssociation of Pb, As, Ca minerals in the glaze layers.

However, these particles are not exclusively associated with the remnant cobalt minerals in this band, and are more clearly visible as individual crystals throughout the glaze, see Figure 19 (spectra 1-9 in Table 6a). As previously observed by Zucchiatti *et al.* (2006), the calcium-lead arsenate particles tend to be acicular in shape. These particles

were formed both in random orientation in the glaze matrix itself (Figure 19c), and at the curved surface of gas bubbles in the glaze, where the rather flat acicular form is most clearly seen up to *c.* 30 μm in length and up to 5μm across (Figure 19d). It would appear that these characteristically shaped crystals are the reaction product between the diffused As and the Pb/Ca, which are components of the glaze mixtures, and thus were precipitated from the molten glaze as a by-product of the chemistry of glazing. Some Ca/As/Pb particles are also present as small globules, presumably once molten (Figure 16 spectra 1 and 9).

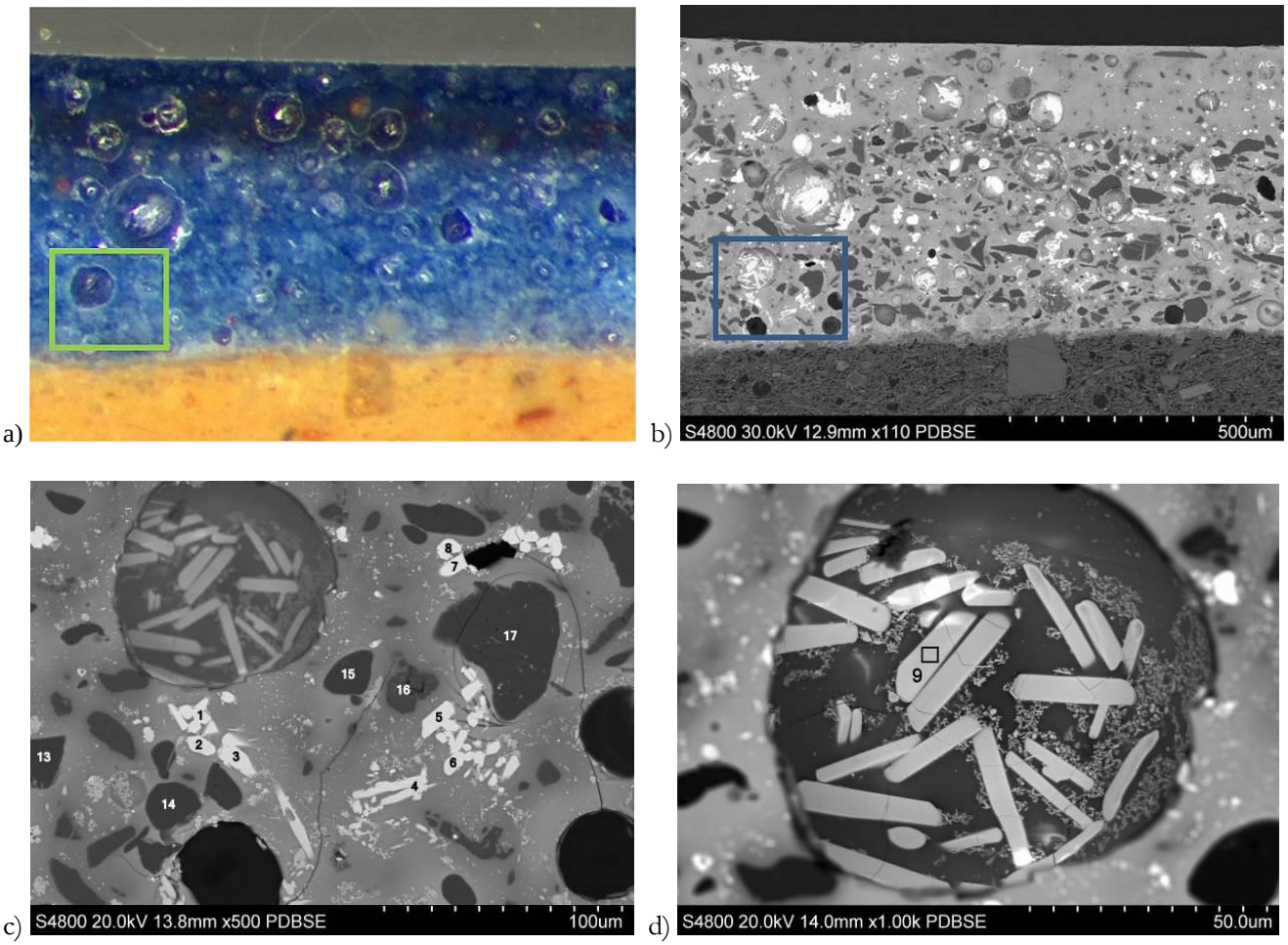

Figure 19. Sample TW01: a) & b) areas outlined in which large calcium-lead arsenate crystals (30μ long) and mineral grains are found in the lower glaze c), detail d) note also the tiny tin oxide particles adjacent to the large arsenate crystals.

Table 6a. Large calcium lead arsenate crystals (white) in Figure 19.

wt% oxides	CaO	As_2O_3	PbO	Atomic % elements	Ca	As	Pb	O
Mean of spectra 1-9	23.0	34.7	42.3	Mean	19.7	16. 9	9.2	54.2

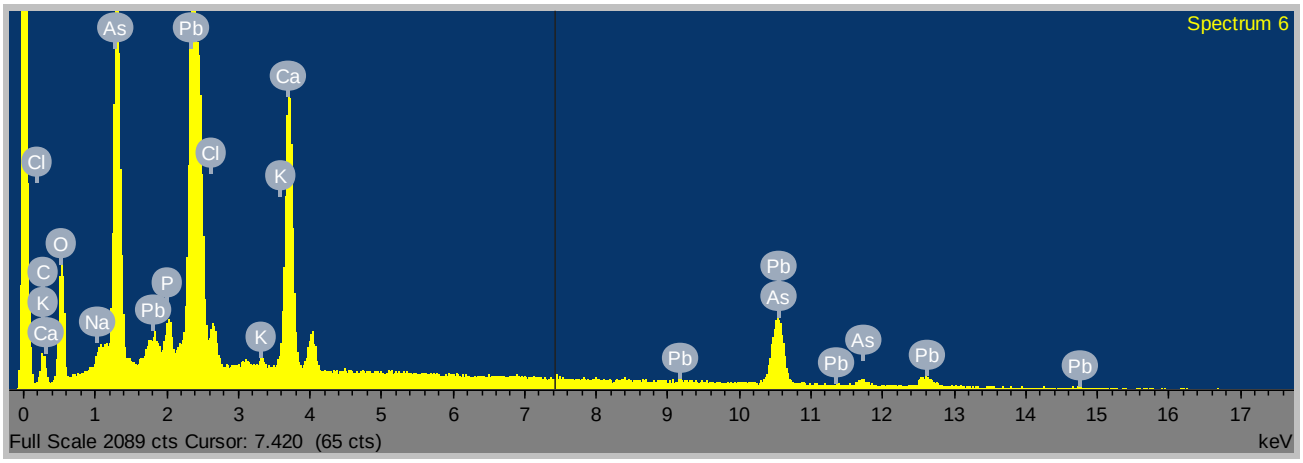

Spectrum 6. Ca, As, Pb. Note the distinguishing large arsenic peak 'La' line at 1.282 keV and smaller 'Kβ1'at 11.724keV.

Table 6b. Larger (dark) mineral grains and associated spectra in the glaze of Figure 19.

Surface minerals wt% oxide	Si	K	Al
Spectra 13-15 & 17 mean. Quartz	99.9	0.0	0.1
Spectrum 16. Feldspar	64.0	13.2	19.1

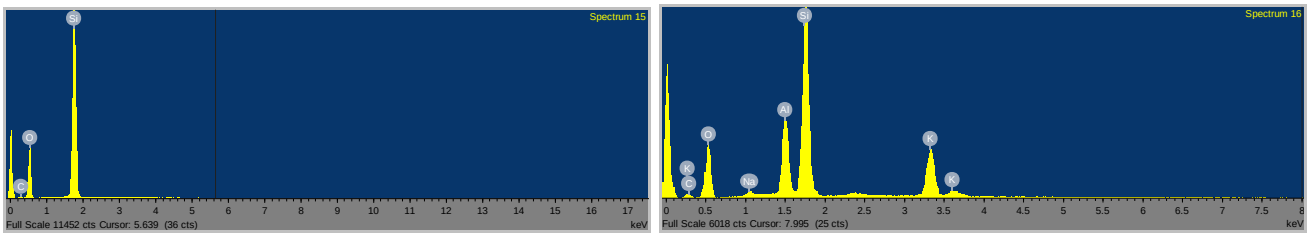

Figure 20. TW01, quartz and feldspar spectra from Table 6b, spectrum 15. Left: Si, O (quartz). Note how 'clean' the spectrum is from this 20 μm size quartz grain, with no beam penetration scatter effects from the glass matrix as the whole beam is fully 'captured' within the confines of the grain. Right: spectrum 16, feldspar grain containing only K, Al, Si, O.

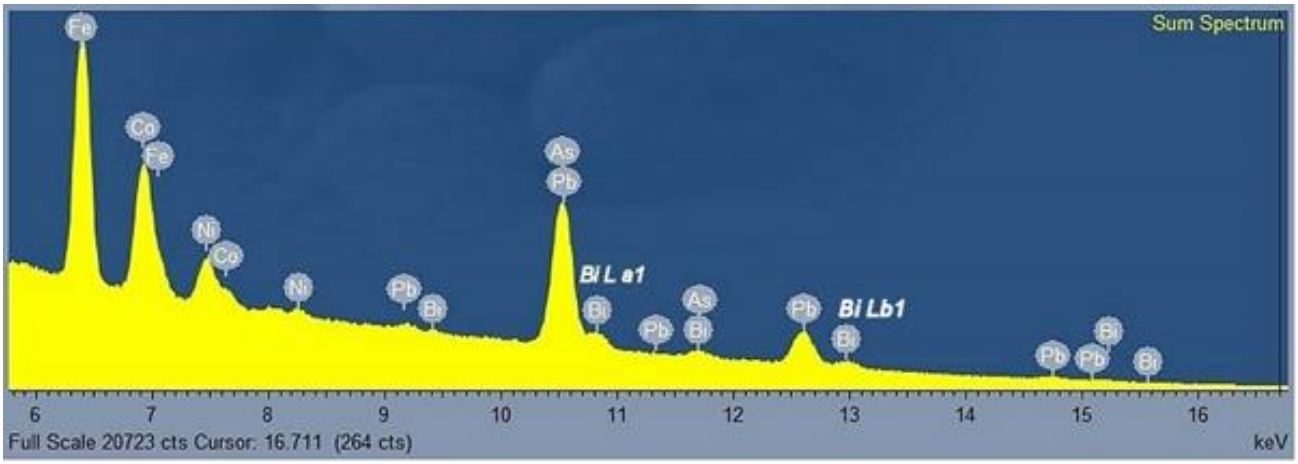

Figure 21. TW01: map sum spectrum - detail of bismuth X-ray energy line peaks, particularly the unique Bi Lα1 and Lβ1 lines.

Other individual mineral grains analysed within the glaze in Figure 19 are of quartz and feldspar that give very specific spectral signatures (Table 6b, and Figure 20 spectra 15 and 16 respectively). These mineral grains are clearly seen in the Si, Al, K elemental maps of Figures 8 and 9, particularly within the opacified lower glaze. The quartz and feldspar result from the addition of sand to the fritted glazing mixture.

Bismuth

Bismuth (Bi) appears in the glaze analyses and the sum map spectra: EDX principal X-ray emission line peaks of bismuth, Bi Lα1 @ 10.838 keV and Bi Lβ1 @ 13.023 keV (Kortright and Thompson 2001) (Figure 21). This line is unique to bismuth and does not overlap with lead or arsenic, whereas some other 'L' line peaks do. These Lα1 and Lβ1 line peaks confirm the presence of bismuth in significant amounts. Bismuth is most likely a contaminant along with arsenic in the cobalt ore (Zucchiatti *et al.* 2006). It was not possible at this moment to provide an element map for bismuth, but further investigation might provide one.

CONCLUSIONS

The combination of detailed digital SEM-EDX high-resolution elemental X-ray maps of polished cross sections, combined with high-resolution FE-SEM imaging and analyses, along with colour optical microscopy images of the maiolica bodies and complex glazes, has extended our ability to identify the phases and minerals present in the paste and glaze and to understand the reactions that have occurred during the two-phase glaze production. Presentation of these data from complex ceramics as colour concentration maps with associated mineral spectral analysis and BSE grey level images provides important visualisation of the minerals in the fabric - spatially, qualitatively and quantitatively.

In summary, the strengths of this technique are visible in the investigation of both maiolica body and glaze, which allowed us to examine in detail:

1) the mineral phases of the maiolica body present in the clay, which are identifiable by mapping and microanalysis together with their morphology, size and distribution seen in BSE images; this information has the potential for a more general application to identify and group ceramic objects made from clay from the same source (i.e. provenance studies);
2) the clay particles within the paste, which show typical vitrification within glassy filaments that form through fusion to the mineral phases (here the potential for further studies using high-resolution microscopy and microanalysis of the glassy filaments and observation of their relationship with clay particles and minerals is proven); and
3) the distribution of the calcium aluminium silicate phases formed as a result of the reaction between the clay minerals and the calcite present in the original calcareous clay is established for the maiolica.

Similarly, the analyses of the maiolica glazes provide detailed information on:

1) the mineral phases present in the sand added to the fritted glazing mixture (quartz and feldspars) in the primary glazed layer, and their absence in the overlying, *coperta* glaze layer. The compositional maps help considerably in the identification of the complexity and distribution of the various high atomic number phases visible in the high-resolution SEM BSE images of the glaze (i.e. phases appearing relatively bright or white in the images). Thus, the tin oxide particles that provide the opacification can be seen as sub-micron particles grouped in larger assemblages and distinguished from both the remnant particles of cobalt pigment and the calcium lead arsenate particles and confirmed from elemental map concentrations and subsequent analyses of the phases extracted from the map data;
2) the cobalt blue glaze colouration, and the association between cobalt, arsenic, nickel and iron is established, much of which has been retained in the remnant pigment mineral particles in a band at the interface between the two glaze layers where the particles of finely ground crushed ore were added to the surface of the first glaze and then overfired with the second transparent glaze. The cobalt has diffused from the pigment ore particles throughout both of the glaze layers along with nickel in equivalent proportions, whereas the iron diffusion remains largely concentrated in the middle-banded region. This information, as well as the presence of arsenic, is crucial in identifying the Erzgebirge region in Saxony as the probable source of the cobalt pigment (Zucchiatti *et al.* 2006, 148; Tite 2009, 2077); and
3) the arsenic distribution (a contaminant of the cobalt mineral) which has similarly diffused throughout the outer and inner glaze layers during glaze firing, but is also present in

specific acicular calcium/lead arsenate crystalline form in both of the glaze layers as a by-product of glazing chemistry.

The ability to revisit primary data using off-line processing software from the original digital EDX analytical system is essential to enhance our interpretations and answer new questions. More recent developments in SEM-EDX mineral identification software are available as the technology develops from more general geological applications (https://nano.oxinst.com/application-detail/geology-petrology-and-mining/).

Element legend

O oxygen
Na sodium
Mg magnesium
Al aluminium
Si silicon
K potassium
Ca calcium
Ti titanium
Mn manganese
Fe iron
Co cobalt
Ni nickel
Sn tin
Pb lead
As arsenic
Bi bismuth

References

Freestone, I. C. 1982. Applications and potential of Electron Probe Micro-Analysis in technological and provenance investigations of ancient ceramics. *Archaeometry* 24, 2, 99-116.

Goldstein, J., Newbury, D. E., Joy, D. C., Lyman, C. E., Echlin, P., Lifshin, E., Sawyer, L. and Michael, J. R. 2003. *Scanning Electron Microscopy and X-Ray Microanalysis. Third edition*. Springer.

Goldstein, J. I., Newbury, D. E., Michael, J. R., Ritchie, N. W. M., Scott, J. H. J and Joy, D. C. 2018. *Scanning Electron Microscopy and X-Ray Microanalysis. Fourth edition.* Springer.

Kortright, J. B. and Thompson, A. C. 2001. X-Ray Emission Energies, in Thompson, A. C. and Vaughan, D. (eds.), *X-Ray Data Booklet*, section 1.2 X-Ray Properties of the Elements, Center for X-ray Optics and Advanced Light Source, Lawrence Berkeley National Laboratory. https://physics.uwo.ca/~lgonchar/courses/p9826/xdb.pdf

Lyman, C. E., Newbury, D. E., Goldstein, J., Williams, D. B., Romig Jr., A. D., Armstrong, J., Echlin, P., Fiori, C., Joy, D. C., Lifshin, E., and Peters, K. R. 1990. *Scanning Electron Microscopy, X-Ray Microanalysis, and Analytical Electron Microscopy: A Laboratory Workbook*. Springer.

Meeks, N. D. 1988. Backscattered electron imaging of archaeological material. In Olsen S. L. (ed.) *Scanning Electron Microscopy in Archaeology*. BAR International Series 452, pp. 23-44.

Molera, J., Pradell, T., Salvadó, N. and Vendrell-Saz, M. 1999. Evidence of Tin Oxide Recrystallization in Opacified Lead Glazes. *Journal of American Ceramic Society* 82, 2871-2875.

Oxford Instruments Nanoanalysis *Application Notes*:
https://nano.oxinst.com/campaigns/downloads/large-area-eds-mapping-phase-distribution-in-archaeological-samples
https://nano.oxinst.com/application-detail/geology-petrology-and-mining/
https://nano.oxinst.com/products/aztec/aztecmineral

Piccolpasso, C. *ca.* 1557. *Li tre libri dell'arte del vasaio.* Italy, Castel Durante (now Urbania), Treatise on maiolica, Victoria and Albert Museum no. MSL/1861/7446, folio 14 recto.

Russ, J. C. 2013. *Fundamentals of Energy Dispersive X-Ray Analysis: Butterworths Monographs in Materials.* Butterworth-Heinemann.

Statham, P. J. 1998. Recent Developments in Instrumentation for X-Ray Microanalysis. In Love, G., Nicholson, W.A.P. and Armigliato, A. (eds.) Modern Developments and Applications in Microbeam Analysis. *Mikrochimica Acta Supplement, vol 15*. Springer, Vienna.

Tite, M. S., Freestone, I., Mason, R., Molera, J., Vendrell-Saz, M. and Wood, N. 1998. Lead glazes in antiquity - methods of production and reasons for use. *Archaeometry 40*, 241-260.

Tite, M. S. 2009. The production technology of Italian maiolica: a reassessment. *Journal of Archaeological Science 36(10),* 2065-2080.

Tite, M. S. 2012. Italian Maiolica. *The Old Potter's Almanack, Volume 17 (2)*, December 2012.

Zucchiattiz, A., Bouquillon, A., Katona, I. and D'Alessandro, A. 2006. The 'della Robbia blue': A case study for the use of cobalt pigments in ceramics during the Italian Renaissance. *Archaeometry* 48(1), 131 – 152.

Further reading

Peruzzo, L., Fenzi, F. and Vigato, P. A. 2011. Electron backscatter diffraction (EBSD): a new technique for the identification of pigments and raw materials in historic glasses and ceramics. *Archaeometry* 53(1), 178-193, Wiley Online Library.

Procop, M., Hodoroaba, V. D., Bjeoumikhov, A., Wedell, R. and Warrikhoff, A. 2009. Improvements of the low-energy performance of a micro-focus x-ray source for XRF analysis with the SEM. *X-ray Spectrometry 38(4)*, 308-311.

Williams, D. B., Goldstein, J. I. and Newbury, D. E. (eds.). 1995. *X-Ray Spectrometry in Electron Beam Instruments*, Plenum Press, NY.

Stokes, D. J. 2008 *Principles and Practice of Variable Pressure/Environmental Scanning Electron Microscopy (VP-ESEM)*. John Wiley & Sons, Ltd.

X-ray Emission Energies: https://www.horiba.com/fileadmin/uploads/Scientific/Documents/XRay/emission_lines.pdf

OBITUARY

We are heartbroken to announce the passing of our friend and colleague Roberta Tomber on the 1st May 2022.

After completing her PhD in 1988, Roberta worked for the Museum of London Archaeology Service (1988–2001) and in the Department of Archaeology, University of Southampton (2002–2004). Her numerous and important publications on Roman ceramics in Britain include *The National Roman Fabric Reference Collection* (https://www.romanpotterystudy.org.uk/nrfrc/base/index.php). A leading scholar in the field of ceramic petrology, Roberta was Acting President of The Ceramic Petrology Group (1999–2012).

She was Honorary Visiting Researcher in the Department of Conservation and Scientific Research (which later became the Department of Scientific Research) in the British Museum (2002–2022). Roberta had a special research interest in Mediterranean and Indian Ocean contacts and exchange between the 1st century BCE and 6th century CE, with numerous publications on ceramics and trade in and between North Africa, the Levant, the Red Sea, South Arabia, Mesopotamia, the Gulf and India. The international reach of her research collaborations and friendships are remembered by colleagues from the Polish Centre of Mediterranean Archaeology Berenike (Red Sea, Egypt) project (https://pcma.uw.edu.pl/en/2022/05/05/roberta-s-tomber-1954-2022-a-memory-by-iwona-zych/) and the Kerala Council for Historical Research (https://kchr.ac.in/archive/275/Dr-Roberta-Tomber-1954-1st-May-2022.html).

In the Department of Scientific Research, she is remembered for her friendship and generous advice to colleagues and students. In the Department she recently co-edited a special issue of the *Journal of Archaeological Science: Reports* on *Contextualising science: Advances in ceramic production, use and distribution* (https://www.sciencedirect.com/journal/journal-of-archaeological-science-reports/vol/16/suppl/C).

Ross Thomas (Department of Greece and Rome, The British Museum) and Michela Spataro (Department of Scientific Research, The British Museum)

CONFERENCE DIARY

43rd International Symposium on Archaeometry in Lisbon, Portugal, 16-20 May 2022

For info:
https://www.isa2020-lisboa.pt/index.php

28th EAA Annual Meeting in Budapest, Hungary, 31 August - 3 September 2022

For info:
https://www.e-a-a.org/eaa2022

Annual Meeting of the Ceramic Petrology Group, Ghent University, 11-12 November 2022

For info:
https://www.ugent.be/lw/archeologie/en/news-events/events/cpg-meeting-2022

THE OLD POTTER'S ALMANACK

The Old Potter's Almanack is the joint letter of the Ceramic Petrology Group and the Prehistoric Ceramics Research Group. It is a venue for presenting current projects, research, reviews, information and topics of interest on all aspects of pottery, ceramics and refractory materials to the audience of scholars, experts, students, interested groups and individuals. The OPA is now published on-line with Heidelberg University and reaches a world-wide audience (see below for website link).

We welcome contributions focussing on any aspect of ceramics technology from any period, culture and geographic locality. Topics can cover materials from collections, museums, excavations and experimental work.

The deadline for copy of articles for the next issue of the OPA is 31st October 2022 (guidelines for contributors are available from the Editor). Copy and other information, news and events should be sent to the Editor, Michela Spataro (for details see below).

Hon. Editor of the OPA
Michela Spataro
Department of Scientific Research
The British Museum, London WC1B 3DG
Email: michelaspataro@yahoo.co.uk

Ceramic Petrology Group (CPG) Hon. President
Patrick Quinn
UCL Institute of Archaeology
31-34 Gord
on Square, London WC1H 0PY
Email: patrick.quinn@ucl.ac.uk

Ceramic Petrology Group (CPG) Hon. Secretary
Silvia Amicone
University of Tübingen, Competence Center Archaeometry – Baden-Wuerttemberg
Mathematisch-Naturwissenschaftliche Fakultät
Eberhard Karls Universität Tübingen
Wilhelmstr. 56, D-72074 Tuebingen
E-mail: silvia.amicone@uni-tuebingen.de

Production Editor of the OPA
Nigel Meeks
Department of Scientific Research
The British Museum, London WC1B 3DG
Email: nmeeks@britishmuseum.org

Prehistoric Ceramics Research Group (PCRG) President
Grace Jones
Bournemouth University, Fern Barrow, Poole, Dorset, BH12 5BB, United Kingdom
Email: gjones@bournemouth.ac.uk

Prehistoric Ceramics Research Group (PCRG) Treasurer
Sarah Percival
NPS Archaeology, Scandic House
85 Mountergate, Norwich NR1 1PY
Email: sarah.percival@nps.co.uk

Prehistoric Ceramics Research Group (PCRG) Secretary
Elina Brook
Wessex Archaeology
Portway House, Old Sarum Park
Salisbury SP4 6EB

WEBSITES

The Old Potter's Almanack
https://journals.ub.uni-heidelberg.de/index.php/opa/index

Ceramic Petrology Group
https://independent.academia.edu/CeramicPetrologyGroupCPG

Prehistoric Ceramics Research Group
https://www.prehistoricpottery.org/